Catena 217 (2022) 106453

Contents lists available at ScienceDirect

Catena

journal homepage: www.elsevier.com/locate/catena

Insight into the carbonaceous fraction of three cultural layers of different age from the area of Verona (NE Italy)

Mara Bortolini [a,*], Federica C. Agnoletto [a], Elena Argiriadis [b], Cristiano Nicosia [c], David B. McWethy [d], Yannick Devos [e], Angela M. Stortini [f], Maela Baldan [g], Marco Roman [a], Tiziano Vendrame [h], Raffaella Scaggiante [h], Brunella Bruno [i], Giulio Pojana [g], Dario Battistel [a,b]

[a] Department of Environmental Sciences, Informatics and Statistics, Ca' Foscari University of Venice, Via Torino, 155, 30172 Venezia Mestre, Italy
[b] Institute of Polar Science – National Research Council CNR-ISP
[c] Department of Geosciences, Università di Padova, Via Gradenigo 6, Padova, Italy
[d] Department of Earth Sciences, Montana State University, Bozeman, MT, United States
[e] Maritime Cultures Research Institute, Vrije Universiteit Brussel, Brussels, Belgium
[f] Department of Molecular Sciences and Nanosystems, University Ca' Foscari of Venice, Via Torino, 155, 30172 Venezia Mestre, Italy
[g] Department of Philosophy and Cultural Heritage University Ca' Foscari of Venice, Dorsoduro 3484/d, 30123 Venezia, Italy
[h] Agenzia Regionale per la Prevenzione e Protezione Ambientale del Veneto, ARPAV, Via Santa Barbara, 5/A, 31100 Treviso, Italy
[i] Soprintendenza Archeologia, Belle Arti e Paesaggio per le province di Verona, Rovigo e Vicenza, Piazza San Fermo, 3a, 37121 Verona, Italy

ARTICLE INFO

Keywords:
Cultural layers
Dark Earth
Carbonaceous fraction
Raman Spectroscopy
Radiocarbon dating

ABSTRACT

Cultural layers are deposits resulting from settlement and human activity on natural soil in the past. Materials from past domestic activities that become buried into the soil can be used to reconstruct human impact in a specific area in the past. For instance, humans have used fire for millennia, and charcoal in soils and sediments is applied as evidence of anthropic activity. In this context, assessing the abundance and degradation level of charcoal fragments can clarify anthropic activities in cultural deposits. In European towns, cultural layers with similar characteristics, have been defined as urban "Dark Earth" (UDE) but their age, formation and composition often differ significantly across sites.

This study examined three archaeological sites in Verona, Italy, where UDE layers with similar characteristics have been identified. The primary aim of this research is to understand the anthropogenic influence on the development of UDE layers, by characterizing their geochemistry and the carbonaceous materials. To pursue this goal, we provide a micromorphological description of the sites, evaluate UDE features and the abundance of charred material and characterize the amorphous/crystalline degree through μ-Raman spectroscopy. Bulk material was described in terms of amounts of total organic carbon (TOC), recalcitrant organic carbon (ROC), total inorganic carbon (TIC), and trace element concentration. Radiocarbon dating of charred and humin fractions was performed to clarify the dynamics underlying UDE origin. We investigate the relationship between the different variables analyzed in the UDE layers at each site. Results show that a diverse array of human activities including metal tool and/or ceramic manufacturing were related to the formation of UDE layers. The investigation of carbonaceous fractions highlight differences in soil organic carbon and charred material, both of which are correlated with human influence.

1. Introduction

Ancient human land uses, including land clearance, cultivation and urban activities and residence often result in specific anthropogenic soils and sedimentary deposits. These soils and deposits offer clues into the cultural activities and human-environment interactions that took place at a site over time, providing an archive of past cultural activities. In archaeological research, such deposits are typically referred to as 'cultural layers' (Butzer, 2011, 2008, 1982 see also Alexandrovskaya and Alexandrovskiy, 2000). Cultural layers are often thick (typically > 10 cm), poorly to unstratified, contain large amounts of anthropogenic and organic remains, and exhibit a dark color (i.e., low values and low

* Corresponding author.
E-mail address: mara.bortolini@unive.it (M. Bortolini).

https://doi.org/10.1016/j.catena.2022.106453
Received 21 February 2022; Received in revised form 7 June 2022; Accepted 9 June 2022
Available online 19 June 2022

chromas in the Munsell soil color chart). In many European towns, deposits with these characteristics have been referred to as urban 'Dark Earth' (hereafter UDE) (see Cammas, 2004; David, 2004; Galinié, 2007; Macphail and Linderholm, 2004; Macphail, 1994; Nicosia, 2018; Nicosia et al., 2017; Nicosia and Devos, 2014) and have been interpreted as the outcome of a range of (sometimes superimposed) anthropogenic activities. These include domestic occupation (Wouters et al., 2017), discard of waste and backfilling (Nicosia 2018; Nicosia et al., 2019), and agricultural activities (Devos et al., 2019, 2013), among others. The formation of UDE in Europe typically results from a complex interplay of human land use, settlement changes and natural events. This implies that each UDE is the outcome of a unique sequence of events often involving multiple drivers (Devos et al., 2019; Macphail, 1994; Nicosia, 2018; Nicosia et al., 2012; Wiedner et al., 2015). Deposits similar in appearance have also been observed outside urban areas (see for instance Wiedner et al., 2015). Furthermore, deposits similar to UDE (thick, dark, dispersed archaeological materials), but very different in terms of cultural, chronological, and geopedological milieu were found in South America (Glaser et al. 2001; Glaser and Birk 2012; Woods and McCann 1999, Arroyo-Kalin et al., 2009). These deposits are referred to as 'Amazonian Dark Earths' (ADE). ADE have been associated to human exploitation of the soil since the first studies were conducted (de Souza et al., 2009; Glaser and Birk, 2012; Kern et al., 2017; Macedo et al., 2017; Neves et al., 2003; Schmidt, 2013; Schmidt et al., 2014), but recent research detail how exogenous processes may lead to the natural origin of ADE indicating that pre-Columbian populations were possibly not the sole responsible for their genesis (Silva et al., 2021). Because a diverse array of human activities and environmental processes are responsible for the formation of soils and soil layers, it is often difficult to disentangle the original driver (human versus natural) of different soil layers.

Beside their common features, the specific mechanism of UDE formation is still hotly debated, and the need of a multidisciplinary approach, when studying cultural layers, has been widely remarked (Devos et al., 2017; Paetsch et al., 2017; Vrydaghs et al., 2016; Wiedner et al., 2015 among others). The determination and characterization of combustion residues become essential to clarify the circumstances that lead to the formation of these layers (Alho et al., 2019; de Sousa et al., 2020; Glaser et al., 2000; Theurer et al., 2021). Recent studies proposed residues of biomass burning such as black carbon, char/charcoal and soot/graphite are responsible for the dark color (Glaser et al., 2001; Schmidt et al., 2002; Schmidt et al., 2000). Others report that the presence of carbonaceous particles is related to the agricultural practice of slash-and-burn and land clearance (Dubois and Jacob, 2016; Glikson, 2013). Many European DE layers are located in urban contexts suggesting there may be sources and activities other than land clearance that are related to their origin.

The high abundance of organic carbon in European DE and ADE is often associated with the presence of biochar and charcoal (Dotterweich and Schreg, 2019; Hardy et al., 2017; Hernandez-Soriano et al., 2016; Liang et al., 2010). This could be due to the adsorption of organic carbon onto the charcoal surface (Pignatello et al., 2006) as well as to a larger presence of biomass in charcoal-rich soils (Jeffery et al., 2011). Soil organic matter is defined as the non-living portion of the organic matter used by the soil fauna that convert soil organic carbon to resistant organic molecules (referred to as humic substances) (Baldock and Skjemstad, 2000; Trumbore, 1997). The recalcitrant organic carbon (ROC), is a bio-resistant fraction constituting the organic carbon in soil associated to the humin content (Valladares et al., 2007) or to biomass burning residues (Baldock et al., 2013; Edmondson et al., 2015; Hobley et al., 2016; Zethof et al., 2019). Zethof et al. (2019), for example, reported that ROC detected through smart combustion represents the graphitic fraction in soils. ROC would thus represent a proxy of past burning events and, especially in such deposits, it is potentially linked to the carbonaceous fraction (Baldock et al., 2013; Hobley et al., 2013; Hobley et al., 2016). Despite being a useful clue into the origin of DE layers, the ROC fraction was never determined in DE layers or in archaeological contexts so far (Natali et al., 2020).

Wilson et al., (2008) suggested that in ADE some elements such as Ca, P, Sr, Zn and Cu could be also affected by enrichment processes linked to the burned biomass residues. The same process has been reported in rural European DE, where a correlation between the content of essential elements (Ba, Zn, Mg, Fe, Na, K, Mn, Ca) and high concentrations of charcoal fragments were observed (Wiedner et al., 2015). Some researchers hypothesized that the high fertility of Dark Earth layers could be associated to a specific charcoal nanostructure. Jorio et al. (2012), for example, used Raman spectroscopy to investigate the structural arrangements of carbon atoms in terms of level of order/disorder. In their study they demonstrated that the environmental action induced a transformation in the crystallite size of charcoal, thus enhancing soil fertility. While previous research demonstrated that Raman spectroscopy is a valuable technique to investigate the nanographitic structure of charred material for pre-Columbian ADE and other anthropogenic soils (Cohen-Ofri et al., 2006; Inoue et al., 2017; Jorio et al. 2012; Ribeiro-Soares et al., 2013;de Sousa et al., 2020), it has never been applied to European DE, and is also a novel method for soil science investigation. Raman spectroscopy as well as infrared spectroscopy (Tinti et al., 2015) are suitable and powerful tools to examine the components and features of soils and sediments. Raman spectroscopy is considered a simple tool to investigate the carbon structure as it can display typical spectral types for carbonaceous materials. These features are related to the positions and the relative intensities of the so-called G (1550–1650 cm^{-1}) and D (1260–1360 cm^{-1}) bands, associated to the crystalline and amorphous structure of carbon, respectively (McDonald-Wharry et al., 2013). The ratio between the intensities of the bands (I_D/I_G) indicates the degree of crystalline/amorphous domains in charred materials (Ferrari and Robertson, 2000; McDonald-Wharry et al., 2013; Tuinstra and Koenig, 1970). The differences in I_D/I_G in different charred materials have been proposed to be diagnostic of the precursor of the carbon sample, as I_D/I_G is related to the in-plane crystallite size (L_a) and/or the average distance between the defects of the precursor material (Cançado et al., 2006; Inoue et al., 2017; McDonald-Wharry et al., 2013). Moreover, the ratio between the intensity corresponding to the minimum value between D and G bands (I_V), and I_G (i.e., I_V/I_G), has been proposed as diagnostic of the thermal burning conditions, where higher I_V/I_G values correspond to lower carbonization temperatures (Inoue et al., 2017; Lambrecht et al., 2021; McDonald-Wharry et al., 2013).

In this paper, our primary aim is to investigate the carbonaceous fraction and the geochemical features in order to address the anthropogenic influence in the cultural layers or 'UDE' exposed in three archaeological sites in and nearby the city of Verona (NE Italy), by using a suite of analytical approaches. Chemical data will be interpreted together with soil micromorphological results to avoid inaccuracy in the assessment of the anthropic activities that lead to the formation of UDE. The abundance and distribution of organic carbon and ROC in relation to the deposition depth as well as size distribution and the carbon structure of charcoal fragments associated to biomass burning residues were investigated in detail. It must be noted that, while charcoal counts are widely used in lacustrine environments for palaeoecological reconstructions (Whitlock et al., 2010 among others), this approach was not commonly applied in European UDE research. In this perspective, the aim of this study is to investigate the UDE main soil constituents: organic carbon and charred particles. The characteristics of carbon and coal that will be examined are correlated to delineate the possible relationships between these two main parts. While not commonly used, we propose to use spectroscopic techniques and approaches to describe different constituents of soil and better understand their origin. More specifically, we analyze carbon structures using. μ-Raman spectroscopy, allowing for a comparison of UDE layers with Amazonian analogues. The primary goal of our research is to better understand human activities and natural processes that led to the development of UDE layers.

2. Material and methods

2.1. Study sites

The samples analyzed were collected from three distinct cultural layers or UDE. The sample base was specifically chosen so that it featured similarities (i.e., thickness, color, lack of internal stratification, scattered archaeological materials, a comparable geological background) and differences (chronology, duration, urban *vs*. rural context). For this purpose, two neighboring urban archaeological excavations in the central part of Roman Verona (Via San Pietro in Monastero 45° 26′ 42.416″ N, 10° 59′ 48.098″ E – hereafter, SPM – and Via Pigna 45° 26′ 43.241″ N, 10° 59′ 47.898″ E – hereafter VP) were selected (Fig. 1). These excavations featured thick UDE layers dated by material culture to the interval between the 3rd-4th and the 6th-7th century CE (see Nicosia, 2018 – see also ^{14}C dates below), in a context of reuse of Roman-age robbed structures. The third set of samples comes instead from a cultural layer exposed at the recent-final Bronze Age (13th to 12th century BCE based on pottery typology – see Salzani, 1983) site of Castelar di Leppia (45° 24′ 29.312″ N, 11° 8′ 20.891″ E - hereafter CDL), represented in Fig. 1. This site lies in an agricultural area east of the city of Verona. It was abandoned after the Bronze Age, so that after the formation of its cultural layer there was no more anthropic deposition. Although the number of samples collected from CDL was limited, this site gives us the opportunity to account for aging processes in charcoal transformations.

From a geomorphological point of view, the city of Verona lies on three main units: the Adige river conoid which forms a fluvioglacial plane, the digression plan of the Adige river, and the conoids formed by the torrents coming from the Lessini Mountains. The soil is mainly composed of clay and sandy, calcareous and dolomitic gravel, from the fluvial deposition, formed in the Holocene (ARPAV, 2005).

2.2. Field description and sampling

Field description of the sites is reported in **Table S1**. Undisturbed blocks for soil micromorphology were collected from the exposed stratigraphic profiles to obtain thin sections. Aliquots for the analysis were later obtained from the undisturbed blocks in the laboratory. Fig. 2 shows the location of the collected blocks and the points where the subsamples were obtained. The amount of material to subsample was calibrated to ensure the maximum integration between all analytical techniques. At VP, the sampled sequences VP I and VP II intercepted the same portion of stratigraphy. A mortar floor was in fact the marker layer allowing to correlate the two sequences. Above this floor a 20–25 cm layer of very charcoal-rich UDE was sampled.

The SPM profile contains two parallel series of samples (SPM I and II), and the UDE layer can be divided in two parts. The lower one

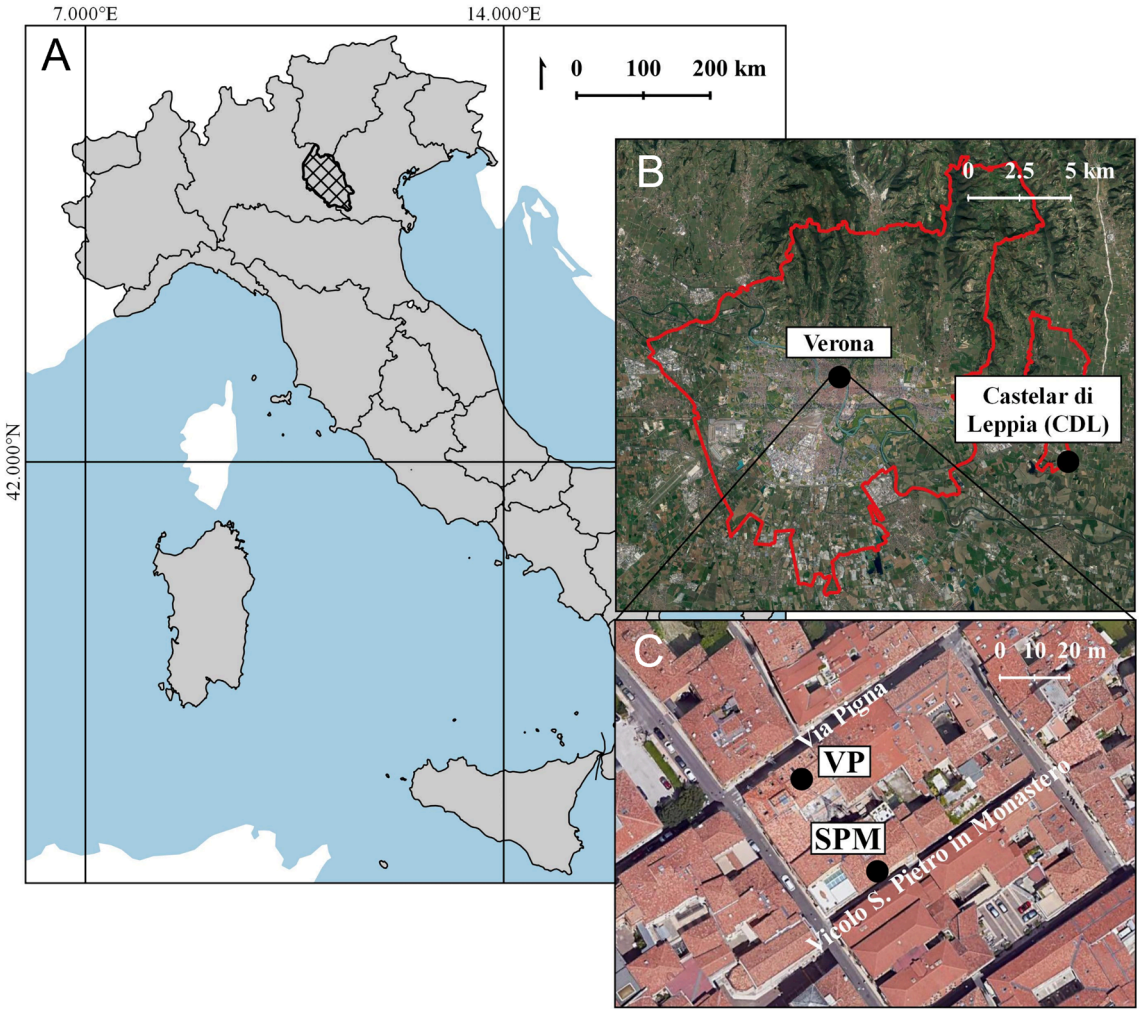

Fig. 1. Location of the sampling sites. The Province of Verona is represented with black hashed lines in the first graph (A). (B) Red contour lines represent the border of the cities of Verona and Lavagno (where the site CDL is located). (C) SPM and VP sites are in the Roman Verona. The figure was created using the Free and Open-Source Geographic Information System (QGIS). Free vector and raster map data at naturalearthdata.com. Google Satellite basemaps were used for the satellite views. (For interpretation of the references to color in this figure legend, the reader is referred to the web version of this article.)

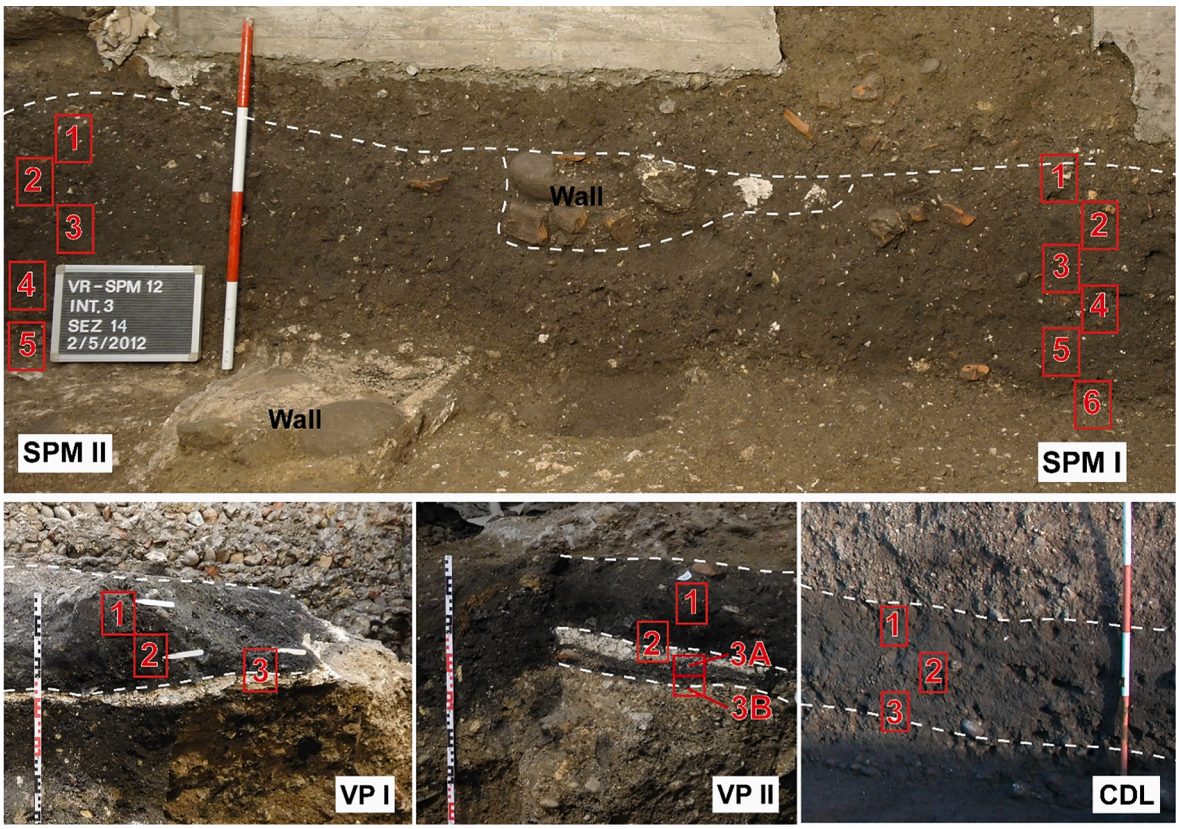

Fig. 2. Profiles of sampling of the blocks for the preparation of the thin sections. From the blocks top, bottom or bulk aliquots were collected to perform the analysis.

accumulated before the construction of a wall, and is incised by an infant tomb containing an African amphora fragment dated between the 3rd-4th and the 6th-7th century CE. The upper UDE formed after the demolition and the levelling of the wall and was truncated in its uppermost part due to later constructions. At CDL a ca. 40 cm-thick very dark gray cultural layer was sampled. This derives from the welding of two anthropogenic layers, that are separated west of the sampled sequence by the wide earthen rampart that surrounded the site during the Bronze Age.

2.3. Soil micromorphology

Thin sections (60 × 80 mm) were prepared from air-dried undisturbed blocks following the laboratory procedures of Beckmann (1997) and described using the terminology of Stoops (2003). Thin sections were studied in plane polarized (PPL) and cross polarized (XPL) transmitted light with magnifications ranging from 12.5x to 400x. From the block samples, a total of 21 thin sections were produced and observed: 6 from the profile SPM I, 5 from the profile SPM II, 3 and 4 from the profiles VP I and VP II respectively, and 3 from CDL sampling site.

2.4. Radiocarbon dating

Bulk samples and charred fragments were sent to Beta Analytics Laboratories (Miami, FL, USA). They provided the humin fraction extraction from the total soil carbon using acid-alkaline treatment from 5 top aliquots from SPM II soil samples. The procedure consists of first sieving of the soil, then acid treatment is performed to remove carbonates, the solution is thoroughly washed, and followed by an alkali treatment aiming to solubilize humic fraction. The alkali-insoluble fraction is the humin fraction ready to be dated. From the same profile (i.e., SPM II), 3 charcoal fragments were hand-picked for radiocarbon dating. Both humin fraction and charcoal fragments were analyzed through Accelerated Mass Spectrometry at the Beta Analytics Laboratories (Miami, FL, USA). Conventional Radiocarbon Ages (CRA) were calibrated using BetaCal4.20: HPD method: INTCAL20.

2.5. Organic, inorganic and recalcitrant carbon

The total organic carbon (TOC), recalcitrant organic carbon (ROC) and total inorganic carbon (TIC) were determined through a Soli TOC Cube (Elementar, Langenselbold, Germany). The method employed (DIN 19539:2016–12) consists of a temperature ramp from 150 °C to 900 °C, using oxygen and nitrogen as reactive and carrier gas, respectively. The dry combustion of TOC occurs between 150 and 400 °C, while ROC is combusted between 400 and 600 °C and TIC is later released up to 900 °C.

2.6. Charcoal counts

The quantification of charcoal fragments was carried out in three aliquots of each sample (~0.5 g). The soil was soaked in a deflocculant solution (technical grade sodium hexametaphosphate 10% and sodium hypochlorite, Merck, St. Louis, MO, USA) for 24 h and then gently washed through a series of nested sieves (mesh opening sizes of 1 mm, 500, 250, 125 and 63 μm) (Whitlock and Larsen, 2002). Dimensional classes are below referred to as CHARx, where × could be 1000, 500, 250, 125 or 63 corresponding to the mesh opening size in μm. Fractions were stored in demineralized water at room temperature until observation. The counting of charcoal particles was performed with a stereomicroscope Olympus SZ61on gridded Petri dishes (Enache and Cumming, 2006; Kirchgeorg et al., 2014; Mustaphi and Pisaric, 2014). All samples were analyzed in triplicate. Larger carbon fragments were isolated for μ-Raman analysis.

2.7. Raman spectroscopy

A total of 29 samples (16 from SPM, 10 from VP and 3 from CDL) among the larger (>1 mm) charcoal fragments were selected for μ-Raman analysis. Samples were mechanically cleaned using scalpels and brushes to expose a fresh surface. All Raman spectra were acquired with an i-Raman 785 s by BWTek (Newark, DE, USA), with a dedicated optical microscope BAC151B Raman Video Microsampling System equipped with a 20X objective, connected by means of optical fibre (1.5 m length) ending in a BAC102 Raman Trigger Probe equipped with a standard 304SS shaft mounting a flat quartz window. The Rayleigh radiation was blocked by a notch filter and the backscattered Raman light was dispersed by a holographic grating on a TE Cooled Linear 2048 pixels CCD Array (cooling temperature: 10 °C); the entrance slit width was fixed at 25 μm. The laser excitation source consists of a 785 nm diode whose power was modulated (1% steps) in a power range from 3 to 300 mW to avoid thermal effects on the analyzed sample. Precisely, the spectra were collected at a power range between 7 and 15 mW, in the 175–3000 cm^{-1} spectral range, with a nominal spectral resolution of 4.5 cm^{-1} and with typical integration times of 60 s. In order to improve the signal-to-noise ratio, five accumulation cycles were collected for each spectrum. Flat and clean surface portions were accurately selected by means of the microscope camera and each sample was characterized by analyzing 2 to 4 surface points. All raw Raman spectra were then deconvolved to identify the position and intensity of the bands according to methodologies proposed by Inoue et al. (2017) and McDonald-Wharry et al. (2013). Each spectrum was cut, selecting the range between 900 and 1800 cm^{-1}, where most of the typical carbon features are located (Dennison and Holtz, 1996; Ferrari and Robertson, 2000; McDonald-Wharry et al., 2013), linear baseline correction was employed selecting the minimum between 900 and 1000 cm^{-1} and 1600–1800 cm^{-1} as anchor points (Inoue et al., 2017). All raw Raman spectra were deconvolved, using Gaussian function, to identify the position and intensity of the most relevant bands (**Figure S1**): eight bands (from lower to higher values of Raman shift: S_L, S, D_S, **D**, A_1, A_2, $\mathbf{G}_G$ and G_L) have been selected and identified (Inoue et al., 2017; McDonald-Wharry et al., 2013).

2.8. Scanning electron microscopy (SEM)

This analysis was carried by isolating particles of interest and sticking them manually to a carbon conductive tape. SEM and energy dispersive spectroscopy (EDS) analysis were performed using a TM3000 tabletop scanning electron microscope (Hitachi, Tokyo, Japan) coupled to an X-ray microanalysis system SwiftED3000 (Oxford Instruments Inc., Bognor Regis, UK). Conditions for recording the EDS spectra were as follows: acquisition time 30.0 s, process time 5 s, accelerating voltage 15 kV.

2.9. Trace elements

The elemental analysis of Fe, Pb, Cu, Mn, Sr, Ba and P was carried out in 4 samples from each SPM and VP, and in 1 sample from CDL. Approximately 0.25 g of homogenized soil samples were microwave digested in 3:1 v/v HCl:HNO_3, adapting the method described in Argiriadis et al. (2021). Trace elements were determined using an Agilent (Palo Alto, CA, USA) MP-4210 MP-AES instrument fitted with a double-pass cyclonic spray chamber and a OneNeb Series 2 nebulizer. The selected wavelengths and MP-AES operating conditions are reported in **Table S3**. Quantification was carried out by 8-points external calibration standards prepared from a mixture of the multi-elemental ICM-103 solution (Ultrascientific), and mono-elemental S and P mother solution. Yttrium was used as internal standard. Results are reported as enrichment factor (EF) calculated using the ratio proposed by Reimann and De Caritat (2000):

$$EF_i = \frac{[i]_{sample}/[Al]_{sample}}{[i]_{ref}/[Al]_{ref}}$$

where *[i]* is the concentration in the sample of the element, the subscript ref indicates the use of Earth's crust concentrations (Rudnick and Gao, 2003) as a reference. Aluminium was used for normalization, because it is assumed to exclusively derive from crustal sources in regional soil contexts (Reimann and De Caritat, 2000).

2.10. Statistical analysis

The pool of data was analyzed using R-studio (version 1.1.463) base packages (version 3.5.1) for statistical hypotheses testing. Pearson correlation coefficients, Wilcoxon-Mann-Whitney and Student's t-tests were used to evaluate the relationship between charcoal and carbon variables (TOC, ROC, TIC, CHAR1000, CHAR500, CHAR 250, CHAR250, CHAR125, CHAR63, G Band and D Band position, I_D/I_G, and I_V/I_G). The Shapiro and Wilk test was used to check the normality of distributions. Variables were compared using the *t*-test or, when the normality hypothesis was not satisfied, using the non-parametric Wilcoxon-Mann-Whitney test.

3. Results and discussion

3.1. Soil micromorphology

Only the most relevant micromorphological traits are discussed here. For the detailed description of thin sections see **Table S2**. In all sequences, specific focus is given to how UDE or cultural layers began to form with respect to the underlying substrates, to identify the origin of the groundmass making up these layers. Second, the degree of expression of syn- and post-depositional processes and transformations that are normally considered as key in UDE formation (i.e., bioturbation, decalcification, cultivation, etc.) is established. Third, the micromorphology of 'black particles' is analyzed. This generic term is used here to describe the complex admixture of charcoal, coal, soot, partially charred plant matter, organic punctuations (*sensu* Stoops 2003) or organic fine substances (Babel, 1975), humified plant matter, etc. that occurs in the fine mass of these deposits. These cannot be differentiated by transmitted light microscopy alone (Canti, 2017), yet they are very prominent in all cultural layers and DE.

3.1.1. Via Pigna (VP)

The base of the sampled sequences is given by a mortar floor (Fig. 3**a**), a typical feature of early medieval dwellings that re-occupy the remains of former Roman structures (see Nicosia, 2018). In profile VP I (sample 3), above this floor there is a 1-cm thick remnant of 'trample' (*sensu* Banerjea et al. 2015). This is particularly important as it shows the micromorphological characteristics of sediments that gradually accumulated *in situ* during the 'life' on this type of floors. These are composed of compacted loam-textured material, particularly rich in wood ash, and contains feces (carnivore/omnivore and herbivore), bone fragments, charcoal, and horizontally-lying articulated phytoliths. These *in situ* sediments are markedly different from the UDE lying above, and the boundary between the two is abrupt even at the microscale (Fig. 3**a**). This suggests a rapid change in the sedimentation, from a trampled domestic context (in VP II for example above the mortar floor there is a clay-lined hearth) to a fast-growing UDE, derived from dumping or backfilling. The UDE is composed of poorly sorted clay loam with randomly distributed archaeological components (charcoal, abundant metal slags and droplets, ceramic material, fecal material). The slags and the droplets confirm the strong presence of metallurgical production activities gathered from trace elements and from the detection of Fe microspheres during sieving (Table 8). The latter are most likely spherical hammerscales (reported in **Figure S6**) produced during

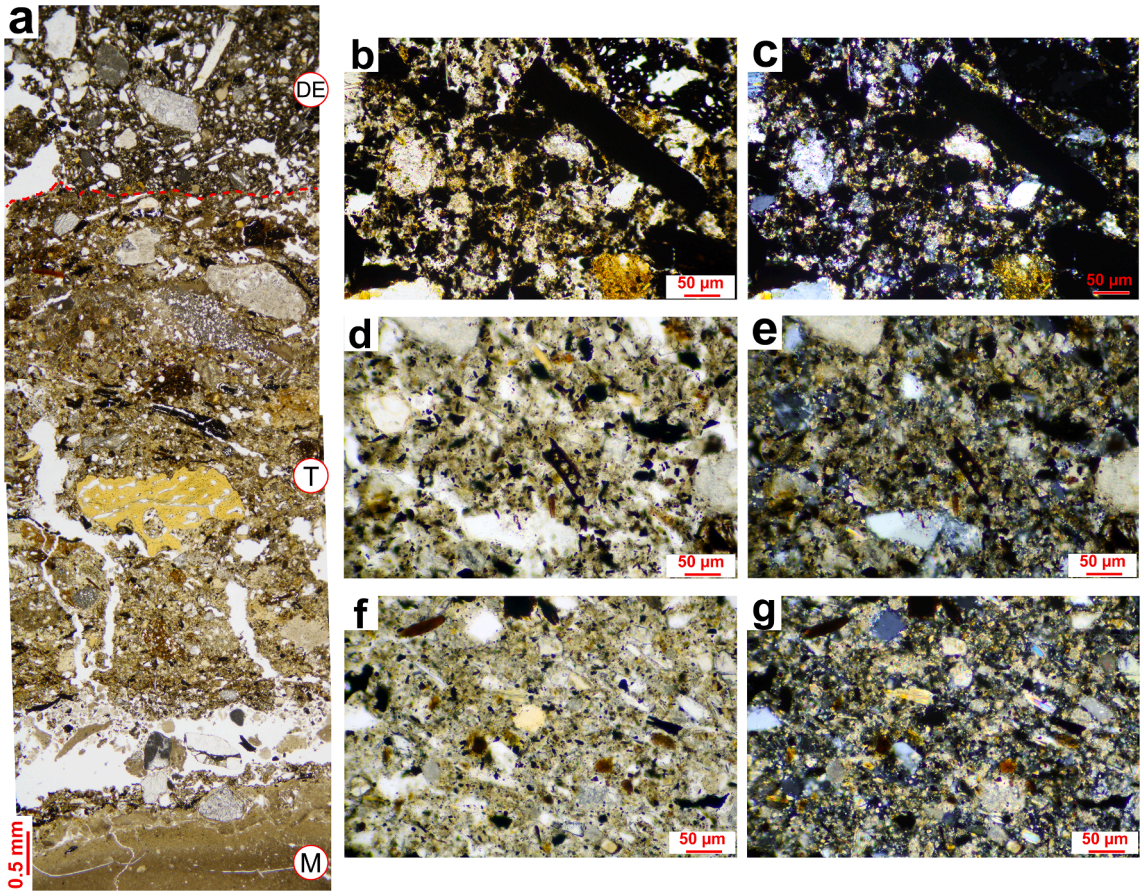

Fig. 3. (a) VPI, sample 1. Contact between mortar floor (M), trample layer (T) and Dark Earth (DE). Note the compositional difference and the abrupt limit (dotted line) between trample accumulated *in situ* and DE resulting from dumping of waste. Note the horizontal alignment of coarser fabric units (bone, rock fragments, charcoal) in layer T. PPL. (b, c) VP I; sample 3. Black particles viewed at 100x with substage condenser inserted. PPL and XPL. (d, e) SPM I, sample 6. Same as above. (f, g) CDL, sample 1. Same as above.

ironworking (Angelini et al., 2017). The slags exhibit a variety of compositions: fayalite in larger (i.e., skeletal) or smaller crystals, portions of amorphous glass with vesicular porosity, amorphous Fe-oxides or dendritic wuestite. Bioturbation in this DE layer is weakly attested and there are no traces of human reworking (i.e., no traces of slaking derived from agricultural practices).

3.1.2. San Pietro in Monastero (SPM)

The UDE lies directly above a layer of levelled construction rubble with a clay-loam matrix, containing Roman-age ceramic. It is interesting to note that this UDE has the same fine-earth matrix (i.e., < 2 mm fraction) in terms of lithology, texture, and quantity of fine 'black particles' of the layer on which it rests. The reworking of older sediments seems therefore to be a key UDE forming factor at SPM and can possibly explain the fact that ^{14}C dating of sediments (i.e., humin fraction) provided older dates than the inclusions they contained (i.e., large charcoal fragments). The UDE collected at SPM contains a randomly distributed admixture of waste from domestic activities (ash, ceramic and bone fragments, carnivore-omnivore excrements, eggshell) with lower quantities of metal slags and droplets from metalworking compared to VP. It is therefore a 'distal facies' of the VP UDE, which instead formed in close proximity to metallurgical activities. The accretion of this DE appears to be fast, as bioturbation is not very expressed. Biogenic channels and earthworm granules are indeed present. Yet, the total biogenic fabric of calcareous Mull-like UDE horizons, observed even in the nearby site of Verona-Via Mazzini 41 (Nicosia 2018) and considered to be one of the key forming factors of UDE (Macphail, 1994, 1981; Sukopp, 1979) are here absent. In SPM profiles there is no evidence of hiatuses in sedimentation, cultivation, or to post-depositional processes such as decalcification. The dumping of heterogeneous material where older sedimentary matrices and older components are mixed with inclusions dating closer to the time of formation seems the most probable explanation for the UDE formation at SPM. This also explains the fact that ^{14}C dates indicate the mixing of sediments (see Table 1 and **Figure S2**).

3.1.3. Castelar di Leppia (CDL)

Soil bioturbation is the main process observable in the Bronze Age cultural layer of CDL. This is evidenced by the strongly expressed channel microstructure, by the presence of crescent-shaped complete infillings ('bow-like features' *sensu* Bullock et al. 1985), loose

Table 1
Conventional Radiocarbon Ages and calibrates ages obtained from the humin fraction and charcoal fragments in SPM II.

Profile	Aliquot	Material	Lab. code	CRA (y BP)	Calibrated date (CE)
SPM II	1 top	humin	580606	1890 ± 30	76–232 (95.4%)
	2 top	humin	580607	1830 ± 30	126–253 (84.4%)
					290–320 (11.0%)
	3 top	humin	580608	1760 ± 30	234–380 (95.4%)
	4 top	humin	580609	1890 ± 30	76–232 (95.4%)
	5 top	humin	580610	1840 ± 30	124–250 (91.6%)
					294–310 (3.8%)
	1 top	charcoal	586538	1820 ± 30	152–256 (69.3%)
					284–326 (22.2%)
	3 top	charcoal	586539	1600 ± 30	416–545 (65.4%)
	5 top	charcoal	586540	1740 ± 30	245–402 (95.4%)

discontinuous infillings of mineral fecal pellets, larger coalescing earthworm droppings, and by scattered earthworm granules. The fine matrix of the cultural layer results enriched in silt-sized calcareous material, giving rise to a crystallitic b-fabric, and in black particles. This contrasts with the local substrate, which is a partially decalcified Cambisol (ARPAV, 2005) formed on the Adige river sediments. The enrichment in calcareous fine material is probably the outcome of mixing processes with sediments derived from lower horizons of this Cambisol, which are still very calcareous. Such mixing derives from the fact that deeper calcareous sediments were dug up (i.e., pits, wells, quarrying of earth material, etc.). The occurrence of black particles probably derives instead from the admixture to the cultural layer of combustion by-products (ash, charcoal, soot, etc.) which have been strongly reworked by bioturbation.

3.1.4. Overall arrangement of 'black particles'

The arrangement and size of black particles in the three sets of samples was determined by observing the groundmass at 100x − 200x magnification and with the use of the sub-stage condenser. Fig. 3 shows: (1) Intimately commixed black particles and mineral material in UDE composed of waste from proximal metallurgical activities (VP I; sample 3, Fig. 3**b, c**) (2) finely (<25 um) comminuted and distanced black particles, some of which still retain the structure of vegetal tissues in UDE derived from ash-rich domestic waste disposal (SPM, sample 12, Fig. 3**d, e**); (3) very finely comminuted black particles in a cultural layer that underwent longer bioturbation (CDL, sample 1, Fig. 3**f, g**). For each site the size distributions of black particles observed in thin sections follow trends in the microcharcoal fragments series.

3.2. Radiocarbon dating

The VP I, VP II, SPM I and SPM II profiles result very close together in terms of location (Fig. 1) and as such they belong to a correlated DE deposit. Stratigraphic correlations, material culture, and ^{14}C dates allow to assume that they encompass the same period. Among them, SPM II provided a larger number of sub-samples, and was selected for radiocarbon dating. Following the indication proposed in Pessenda et al., (2001), the humin fraction of the soil was initially dated as it is, differently from charcoal fragments, potentially less affected by post-depositional processes. Conventional Radiocarbon Ages (CRA) and calibrated ages are reported in Table 1 and **Figure S2**.

As reported in Table 1 and shown in **Figure S1**, the radiocarbon calibrated ages obtained from the humin fraction span a period between 75 and 380 CE (significance corresponding to 2σ). These radiocarbon ages were not chronological, suggesting that the matrix has been mixed and reworked, as also evidenced by the thin section observation. Indeed, the radiocarbon ages do not increase with the increase of the depth, and that is independent of the typology of the fraction of carbon used (i.e., charcoal or humin). A similar sequence of mixed-aged materials was observed in UDE from Brussels (Devos et al., 2017) and Firenze (Nicosia 2018).

Some of the charred fragments hand-picked from the SPM II profile were radiocarbon dated to test the hypothesis of post-depositional events. Calibrated ages obtained from charcoal fragments are reported in Table 1 (see also **Figure S2**). As shown, charcoal calibrated dates ranged from 150 to 545 CE. Looking at the results it is possible to find out slight differences between the radiocarbon dating of charred material versus humin fraction. This difference in the dating between humin and charcoal fractions suggests a possible initial anthropization period resulting in an enrichment of organic matter (during 1st and 2nd century) before the cultural layer (during the 4th – early 6th) was deposited. Humic carbon represents a part of the matrix originally deposited (van der Plicht et al., 2019; van Mourik et al., 2012) and then enriched in coarser fragments and charcoal during the subsequent centuries. Indeed, the humin fraction is also defined as "allochthonous organic carbon", that is the carbon fraction deposited in the matrix prior to the formation of the autochthonous carbon, more easily oxidable, in soil (van der Plicht et al., 2019). The period of formation of UDE in VP and SPM is nearly in line with the DE exposed in the nearby urban excavation of Via Mazzini 41, dating to the late 4th – early 6th century CE (Bruno and Fresco, 2014). The dates obtained at SPM show that in UDE studies it is crucial to define the context of the material being dated. Dated material from an *in situ* UDE or cultural layer dates – roughly– its moment of formation (with all limitations from old wood effect, stocked wood, re-use, heirlooms, etc). Dated material from dumped or remobilized UDE or cultural layers provides us with a *terminus post quem* with respect to the moment in which those sediments were dumped. Hence, from our dating results it is possible to consider radiocarbon dating not only a base technique to date the soil horizons, but also to help evaluate the sequence of human and natural processes responsible for soil layer development and deposition.

3.3. Carbon

The TOC and TIC were determined together with the ROC. The concentration profiles along all sites did not exhibit a particular trend (see **Table S4**). Therefore, the mean concentrations of TOC, ROC and TIC for each profile were considered as reported in Table 2. The highest ROC and TOC mean values were detected in the VP for both the profiles VP I and VP II, while SPM showed a higher TIC.

The means were compared using the *t*-test or, when the normality hypotheses was not fulfilled, using the non-parametric Wilcoxon-Mann-Whitney test. The resulting *p*-value of the tests are reported in Table 3. As shown, TOC, ROC and TIC are not significantly different between parallel profiles from the same sites. Nevertheless, VP has significantly higher values of TOC and ROC in comparison with both SPM and CDL, as well as a depletion in TIC. However, CDL shows significantly lower TOC and ROC than SPM.

Values ranges between 0.9 and 3.3% and are consistent with the concentrations found in other DE horizons all over Europe. Devos et al. (2013, 2017), reported a TOC content between 0.5 and 3.7% in Brussels, while slightly lower organic carbon concentrations were observed in Padua (0.7–1.9%) and in Florence (0.25–1.25%) (Nicosia et al., 2012, 2019). These values were ascribed to the result of handling processes (domestic waste or byre) and manure addition to the soil (Devos et al., 2017, 2013; Wiedner et al., 2015).

Although the three sites are significantly different when compared for TOC, most variability is due to the ROC concentrations, ranging between 0.5 and 1.6% (Table 3). A comparison of ROC between the sites returns the lowest *p*-values, following the same relationship observed for TOC as ROC concentration resulted VP > SPM > CDL (Table 3).

It must be noted that TOC and ROC values are significantly higher in VP than in SPM despite the vicinity of the two sites. This suggests that the horizontal variability in DE, likely related to different practices such as agriculture or waste management, is significant even for short-range distances.

Table 2
Mean values organic (TOC), recalcitrant (ROC) and inorganic carbon (TIC) from two sections at Vicolo San Pietro in Monastero (SPM I and SPM II) via Pigna (VP I and VP II), and from Castelar di Leppia (CDL).

Profile/site	n	TOC (%)	ROC (%)	TIC (%)
SPM I	9	1.3 ± 0.1	0.8 ± 0.1	4.3 ± 0.2
SPM II	10	1.3 ± 0.2	0.7 ± 0.1	4.2 ± 0.2
SPM	19	1.3 ± 0.1	0.7 ± 0.1	4.3 ± 0.1
VP I	6	3.3 ± 3.0	1.6 ± 0.7	3.2 ± 1.2
VP II	6	2.5 ± 1.7	1.5 ± 0.7	3.0 ± 1.5
VP	12	2.9 ± 1.4	1.5 ± 0.4	3.1 ± 0.8
CDL	3	0.9 ± 0.4	0.5 ± 0.1	3.6 ± 0.1

Table 3
Comparison between mean values of organic (TOC), recalcitrant (ROC) and inorganic carbon (TIC). *p*-values obtained using the Student's t or the Wilcoxon-Mann-Whitney. *p*-values < 0.05 (in bold) indicate a significant difference between the means.

	TOC	ROC	TIC
SPM I *vs* SPM II	0.91	0.27	0.65
VP I *vs* VP II	0.55	0.78	0.74
SPM *vs* VP	**0.033**	**0.001**	**0.008**
VP *vs* CDL	**0.009**	**$9\bullet10^{-5}$**	0.18
SPM *vs* CDL	**0.008**	**0.0003**	**$4\bullet10^{-8}$**

3.4. Charcoal

The charcoal content was determined following the procedure proposed by Whitlock and Larsen (2002). After separation into five dimensional classes (1 mm, 500, 250, 125 and 63 μm) the concentration profiles along all the sites did not show any trend (see **Figures S3-S5**). The results of this analysis are reported in Table 4 as means and corresponding confidence intervals (95%) for each profile and site. As shown in Table 4 the number of charcoal fragments increases with the decrease of the dimensional class, for all profiles and sites.

A non-parametric Wilcoxon-Mann-Whitney test was conducted to compare charcoal fingerprint distribution between sites and profiles. The *p*-values reported in Table 5 support the hypothesis that, similarly for TOC, ROC and TIC concentrations, significant inter-site rather than intra-site differences are noted. VP shows the highest abundance of charcoal fragments in all dimensional classes, except for the smallest (63 μm). In addition, VP is the only site where coarser charcoal particles (>500 μm) were detected. CDL exceeds only in CHAR63 with respect to SPM, but this dimensional class is not significantly different from the corresponding class in VP. Results from the thin sections show similar results, suggesting there were different processes involved in UDE formation. The charcoal fingerprint distribution is similar within the profiles from the same site, confirming that in the UDE horizons from Verona, neither trends nor internal differentiations can be highlighted, further supporting the idea that different activities (backfilling and dumping of material mixed with the matrix and sometimes reworked), were responsible for UDE formation.

In particular, VP and SPM show a different fingerprint for TOC, ROC and charcoal distributions, although these two sites belong to UDE deposits that can be correlated. The different charcoal distribution may be associated to distinct dynamics of production and/or transport of the biomass burning residues. This might in turn be related to independent anthropogenic activities that occurred in the specific site (Davidson et al., 2006), such as the metallurgical activities described previously in the section 3.1. A relatively higher concentration of the largest charcoal fraction in VP and absence in SPM could be indicative of a very local source of charcoal and a massive biomass burning input in VP.

Further information about the charcoal inner structure were obtained by μ-Raman spectroscopy performed on the surface of the larger charcoal fragments.

Fig. 4 shows typical Raman spectra obtained from the larger charcoal

Table 4
Mean values of the charcoal counts g^{-1} in samples sieved at 1000, 500, 250, 125 and 63 μm from two sections at Vicolo San Pietro in Monastero (SPM I and SPM II) via Pigna (VP I and VP II), and from Castelar di Leppia (CDL).

Site	n	CHAR1000	CHAR500	CHAR250	CHAR125	CHAR63
SPM I	27	0 ± 0	0 ± 0	2 ± 1	11 ± 4	17 ± 4
SPM II	30	0 ± 0	0 ± 0	3 ± 2	9 ± 3	15 ± 3
SPM	57	0 ± 0	0 ± 0	3 ± 1	10 ± 2	16 ± 2
VP I	18	2 ± 1	3 ± 1	20 ± 8	50 ± 20	60 ± 30
VP II	18	0.5 ± 0.5	2 ± 1	16 ± 7	25 ± 6	45 ± 20
VP	36	1.1 ± 0.6	2.4 ± 0.9	18 ± 5	40 ± 10	50 ± 20
CDL	9	0 ± 0	0 ± 0	0.4 ± 0.4	13 ± 6	80 ± 45

Table 5
P-values for the comparison between mean values of charcoal counts in samples sieved at 1000, 500, 250, 125 and 63 μm. *p*-values obtained using the Student's t or the Wilcoxon-Mann-Whitney test. *p*-values < 0.05 (in bold) indicates a significant difference between the means.

	CHAR1000	CHAR500	CHAR250	CHAR125	CHAR63
SPM I *vs* SPM II	NA	NA	0.97	0.41	0.38
VP I *vs* VP II	0.053	0.89	0.71	0.22	0.80
SPM *vs* VP	**10^{-7}**	**10^{-11}**	**10^{-11}**	**10^{-9}**	**10^{-8}**
VP *vs* CDL	**0.039**	**10^{-3}**	**10^{-5}**	**10^{-3}**	0.059
SPM *vs* CDL	NA	NA	**0.050**	0.25	**10^{-6}**

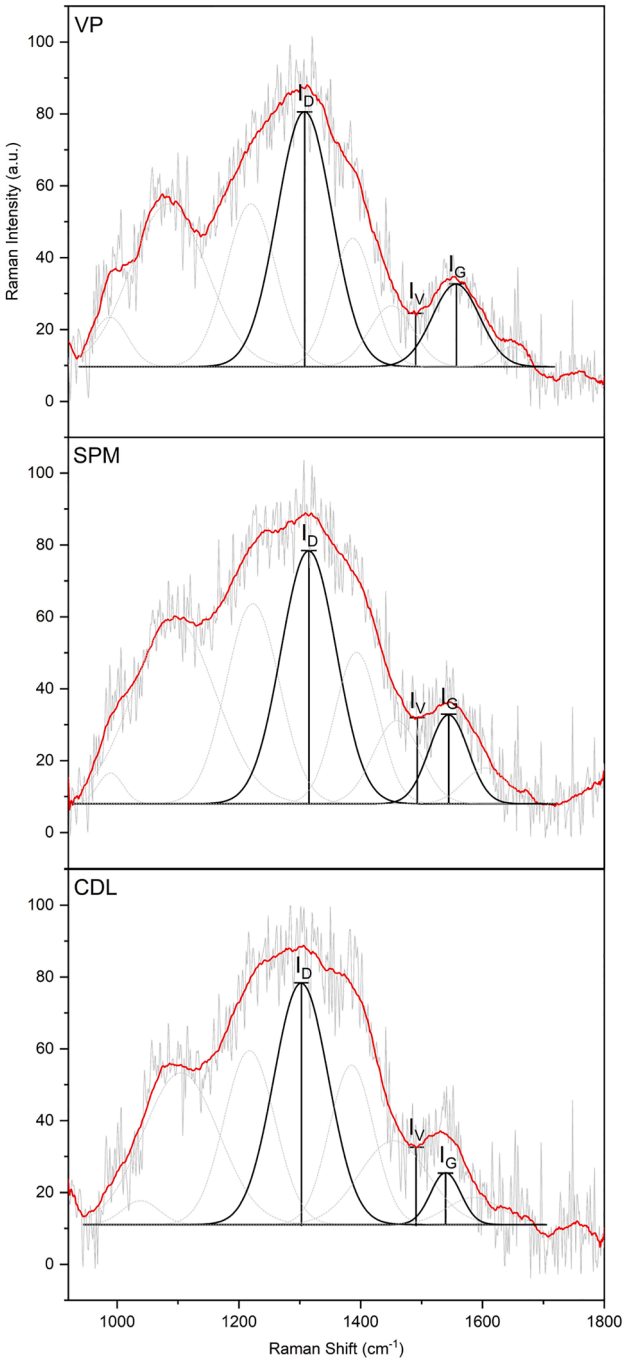

Fig. 4. Typical Raman spectra of the sites analyzed in this study. The spectral features used for interpretation and fitting procedures are highlighted.

fragments collected in the three sites. After deconvolution, all spectra show the typical features of carbon, with D and G bands located at ~ 1350 and ~ 1600 cm^{-1}, respectively (Cohen-Ofri et al., 2006; De de Sousa et al., 2020; Dennison and Holtz, 1996; Dresselhaus et al., 2005; Ishimaru et al., 2007; Jawhari et al., 1995; Kawakami et al., 2005; Tuinstra and Koenig, 1970). In all spectra, the D band shows higher intensity with respect to the G band, suggesting that low level of crystallinity in the inner lattice of the material is present (Ferrari and Robertson, 2004). The Raman spectra of the crystalline graphite show just the G band at ~ 1580 cm^{-1}, but if the symmetry is perturbated (i.e. sp^3 bonding, edges, impurities, etc.) the D band appears and there can be a shift in the G band position (Cançado et al., 2007; Ferrari and Robertson, 2004, 2000; Wang et al., 1990). Indeed, the D band is the evidence of the breathing modes of the sp^2 carbon in rings (Ferrari and Robertson, 2004), this is associated to the presence of some breakdown in the symmetry of the graphite lattice (Wang et al., 1990). The G band is linked to the vibration modes of the sp^2 carbon atoms (Ferrari and Robertson, 2004, 2000).

The main diagnostic parameters obtained from Raman spectra are summarized in Table 6 and are: the positions (cm^{-1}) of D and G bands, the ratios between the intensities of the two bands (I_D / I_G), and the ratios between the intensity of the valley of the two bands and the G band intensity (I_V / I_G), and the in-plane crystallite size (L_a) of charred particles was calculated using the equation proposed by Cançado et al. (2006). L_a is inversely proportional to the ratio between the intensities of D and G bands (Cançado et al., 2007, 2006; Cuesta et al., 1998; Ferrari and Robertson, 2000; Jorio et al., 2012; Tuinstra and Koenig, 1970). Our L_a results are around 50 nm, slightly higher then the Amazonian analogous (Jorio et al., 2012; Ribeiro-Soares et al., 2013) and are much more similar to the graphitic materials studied by Cuesta et al. (1998). A statistical comparison between these parameters was carried out using the Student's *t*-test (or Wilcoxon-Mann-Whitney test). The *p*-values of the test performed within and between the sites are reported in Table 7.

Charcoal fragments structures within the profiles, as well as between the sites of the urban context of Roman Verona (i.e., VP and SPM), do not show significant differences. Conversely, the older site CDL exhibited markedly higher I_V/I_G and lower G-band position values. The G-band feature indicates a higher level of disorder in the charcoal structure in CDL with respect to those in SPM and VP. This finding could be explained by the difference in age, as CDL is likely older than the others. Being older and likely more degraded, charcoal had more disordered structures with a lower fraction of graphitized carbon (Smidt et al., 2020, Smidt et al., 2017). This aging process may be ascribed to environmental factors, such as pH and humidity of the soil, microbial activities or water erosion (Inoue et al., 2017; Rumpel et al., 2015). Interactions of charred residues in soils due to chemical and physical changes have been investigated (Cheng et al., 2008; Inoue et al., 2017). Cheng et al. (2006) suggested that the main changing of charcoal features could be due to physical and biological weathering in soils. Moreover, higher values of I_V/I_G in CDL may be indicative of lower burning temperatures. This evidence suggests that the more ancient charcoal of CDL was produced at lower carbonization temperatures, providing a limited removal of amorphous structures and a scarce formation of graphene-like networks (McDonald-Wharry et al., 2013). On the other hand, the similarity between SPM and VP supports the assumption that SPM and VP are coeval, while higher carbonization temperatures may be related to high-energy demand processes, such as smelting (as previously observed) or ceramic manufacturing.

Table 6
Mean values of the parameters from Raman spectra obtained in charcoal samples from two sections at Vicolo San Pietro in Monastero (SPM I and SPM II) via Pigna (VP I and VP II), and from Castelar di Leppia (CDL).

Site	n	Band G (cm^{-1})	Band D (cm^{-1})	I_D / I_G	I_V / I_G	L_a (nm)
SPM I	4	1557 ± 6	1314 ± 9	1.7 ± 0.3	0.89 ± 0.07	52 ± 8
SPM II	12	1554 ± 2	1314 ± 4	1.7 ± 0.1	0.94 ± 0.04	54 ± 3
SPM	16	1555 ± 2	1314 ± 3	1.7 ± 0.1	0.93 ± 0.03	53 ± 3
VP I	6	1549 ± 6	1318 ± 3	1.9 ± 0.5	0.94 ± 0.11	52 ± 10
VP II	4	1553 ± 4	1316 ± 18	1.9 ± 0.4	0.89 ± 0.28	47 ± 10
VP	10	1551 ± 4	1317 ± 5	1.9 ± 0.3	0.91 ± 0.10	50 ± 8
CDL	3	1542 ± 5	1316 ± 9	1.7 ± 0.4	1.16 ± 0.18	53 ± 10

Table 7
Comparison between mean values of Raman Parameters. *p*-values obtained using the t-Student or the Mann-Whitney test depending on the normality of the distribution previously checked with the Shapiro-Wilk test. *p*-values < 0.05 (in bold) indicates a significant difference between the means.

	Band G (cm^{-1})	Band D (cm^{-1})	I_D / I_G	I_V / I_G	L_a (nm)
SPM I *vs* SPM II	0.13	0.68	0.66	0.10	0.67
VP I *vs* VP II	0.31	0.82	0.78	0.58	0.55
SPM *vs* VP	0.08	0.077	0.19	0.76	0.34
VP *vs* CDL	**0.012**	0.46	0.24	**0.005**	0.42
SPM *vs* CDL	**0.006**	0.48	0.96	**0.019**	0.98

3.5. Metallic droplets and anthropogenic soil

During the microscopy observation of the samples for charcoal analysis, a large number of magnetic spheres were detected in both VP profiles. A deeper investigation of the distribution of these droplets showed that they were most abundant in the > 63 μm fraction (see Table 8).

A representative selection of them were handpicked and analyzed by SEM-EDS to study their morphology and elemental composition. A typical SEM micrograph is shown in **Figure S6.** Such magnetic droplets exhibit a regular spherical shape with a diameter in the 80 to 280 μm range. The elemental analysis of these spheres evidenced that they are mainly composed of iron, aluminum and oxygen (coherently the phases identified during the thin section observation). Ferrous spheres in modern soils have been usually associated to fly ash from metallurgical activities and road dust pollution (Bourliva et al., 2016; Fisher et al., 1978; Howard and Orlicki, 2016; Ngu et al., 2007). To the best of our knowledge, these kinds of structures were never reported before in UDE. The presence of less abundant metallic droplets and of the smallest dimensional class in SPM compared to VP, suggests that the latter might be the source site of the metallic particles, then transported by the wind to the neighboring site SPM. Therefore, VP may have been a localized site for metal smoldering. This interpretation is supported by the abundance of larger charcoal particles that likely derive from the metallurgic activities as well.

The presence of metallic droplets prompted to investigate in detail the elemental composition of the soils for metals and other elements typically associated to anthropogenic soils, such as P. Two samples from each profile (VP I, VP II, SPM I and SPM II) were analyzed together with one sample from CDL. The concentrations are reported in Table 9,

Table 8
Distribution of the ferrous microspheres of different size from the three sites Via Pigna (VP) Vicolo San Pietro in Monastero (SPM) and Castelar di Leppia (CDL).

Site	500 μm > d > 250 μm	250 μm > d > 125 μm	>63 μm
VP	2 ± 1 counts g^{-1}	15 ± 9 counts g^{-1}	30 ± 10 counts g^{-1}
SPM	NA	NA	7 ± 1 counts g^{-1}
CDL	NA	NA	NA

Table 9
Mean values of the Enrichment Factors from two sections at Vicolo San Pietro in Monastero (SPM I and SPM II) via Pigna (VP I and VP II), and from Castelar di Leppia (CDL).

Site	n	EF Fe	EF P	EF Ca	EF Mg
SPM I	2	2.6 ± 0.1	3.6 ± 0.3	30 ± 1	4.1 ± 0.2
SPM II	2	2.6 ± 0.1	3.8 ± 0.0	25 ± 3	4.2 ± 0.4
SPM	4	2.6 ± 0.1	3.7 ± 0.1	28 ± 2	4.2 ± 0.2
VP I	2	10 ± 5	7 ± 1	23 ± 1	5 ± 1
VP II	2	20 ± 13	9 ± 3	40 ± 17	5.9 ± 0.2
VP	4	14 ± 6	8 ± 1	30 ± 8	5 ± 0.5
CDL	1	2	3	18	5

expressed as enrichment factors (EF) as proposed by Reimann and De Caritat, (2000) (concentration values are reported in **Table S5**).

Sutherland (2000) proposed that an elemental concentration should be considered anomalous when its EF exceeds a value of ~ 20. According to this threshold level, all examined UDE profiles were highly enriched in P and Ca, while VP was significantly enriched in Fe. The high value of iron EF in VP is indicative of human forcing processes, as previously suggested by the presence of metallic droplets mostly found in VP soil samples. Although the EF evidenced marked differentiation between the three sites, they show similar values within the profiles of the same site. This feature further supports the occurrence of a horizontal rather than vertical variability in DE deposits. The concentration of P found in UDE is in agreement with the results obtained in similar ancient anthropogenic soils in northern Italy (Migliavacca et al., 2013; Vittori Antisari et al., 2013). Higher P content in all the sites agrees with the presence of anthropogenic soil (Patten et al., 2012), as the presence of P has already be linked to human activities, being associated to excrement and byre addition and/or to the dumping of biomass burning residues (Devos, 2018). In this case, the excess of P in VP might be related to this latter activity. This is in agreement with the charcoal and ROC abundance previously observed. Calcium EF shows a particular increase in VP and SPM, with respect to CDL. Calcium and Manganese can derive from different sources in anthropogenic soils, in the sites of our interest the calcium and magnesium can firstly derive from calcareous-calcarenitic minerals, present in the soil matrix. These could then undergo different processes into the soil thanks to the continuous input of organic material from domestic waste. Humification processes of organic carbon can affect the soil pH, and in acidic conditions dissolution of carbonates can occur (Zamanian et al., 2016). The presence of metallic ions, such as Ca^{2+}, in organic carbon rich soils leads to a series of mechanisms that contribute to the organic matter sorption and stabilization (Barreto et al., 2021; Rowley et al., 2018; Shi et al., 2017). The main mechanisms involve the aggregation and occlusion of soil organic matter with calcium, and parallelly the inclusion of organic matter within $CaCO_3$ minerals (Clough and Skjemstad, 2000; Rowley et al., 2018). The significant presence of P detected in cultural layer samples can also arise from phosphatic minerals, suggesting the significant presence of calcium and manganese. Therefore, the increasing of nutrient in soil where availability of biochar and charcoal have been suggested by Atkinson et al. (2010) Lehmann and Stahr (2007) and Steiner et al. (2007).

3.6. Pairwise correlation

Pearson correlation coefficients between pairs of variables are reported in Table 10. TOC and ROC were significantly and positively correlated (r = 0.60, *p*-value < 0.01). Qi et al. (2017) found positive correlation between TOC and ROC in agricultural and parkland soils, in agreement with our results. From their observations, ROC fraction included condensed pyrogenic carbon, condensed aromatic humic carbon and other non-reactive organic carbon fractions. The ROC can be related to the pyrogenic products that can, in turn, contribute to an increase of the more labile TOC in burial conditions. Therefore, in the context of DE, TOC input may partially derive from the significant

Table 10
Pearson correlation coefficient (p-value) between organic (TOC), recalcitrant (ROC) and inorganic carbon (TIC), dimensional charcoal counts (1000,500,250,125 and 63 μm) and Raman parameters (Band G, Band D, I_D/I_G and I_V/I_G).

	TOC	ROC	TIC	CHAR1000	CHAR500	CHAR250	CHAR125	CHAR63	Band G (cm^{-1})	Band D (cm^{-1})	I_D / I_G	I_V / I_G	L_a (nm)
TOC		**0.60 (<0.01)**	**−0.72 (<0.01)**	0.28 (0.09)	**0.53 (<0.01)**	**0.50 (<0.01)**	**0.52 (<0.01)**	0.21 (0.22)	−0.32 (0.09)	0.24 (0.20)	0.20 (0.30)	−0.16 (0.40)	−0.14 (0.48)
ROC			**−0.65 (<0.01)**	0.36 (0.03)	**0.57 (<0.01)**	**0.55 (<0.01)**	**0.61 (<0.01)**	**0.38 (0.02)**	−0.24 (0.20)	0.39 (0.03)	0.17 (0.37)	−0.02 (0.88)	−0.13 (0.50)
TIC				−0.04 (0.79)	**−0.39 (0.017)**	−0.25 (0.14)	−0.29 (0.08)	−0.20 (0.25)	−0.17 (0.36)	0.35 (0.06)	−0.30 (0.10)	−0.08 (0.67)	0.30 (0.11)
CHAR (1000)					**0.80 (<0.01)**	**0.78 (<0.01)**	**0.84 (<0.01)**	**0.55 (<0.01)**	−0.31 (0.10)	0.25 (0.18)	−0.04 (0.81)	−0.10 (0.61)	0.18 (0.34)
CHAR (500)						**0.81 (<0.01)**	**0.78 (<0.01)**	**0.41 (0.01)**	−0.35 (0.06)	0.22 (0.25)	0.34 (0.07)	−0.10 (0.58)	−0.22 (0.26)
CHAR (250)							**0.92 (<0.01)**	**0.62 (<0.01)**	−0.29 (0.13)	0.19 (0.32)	−0.01 (0.96)	−0.15 (0.41)	0.11 (0.57)
CHAR (125)								**0.72 (<0.01)**	−0.37 (0.04)	0.26 (0.16)	0.03 (0.89)	−0.44 (0.82)	0.07 (0.72)
CHAR (63)									−0.42 (0.02)	0.28 (0.14)	−0.23 (0.23)	0.34 (0.07)	0.26 (0.18)
Band G (cm^{-1})										−0.09 (0.62)	−0.24 (0.21)	**−0.52 (<0.01)**	0.17 (0.37)
Band D (cm^{-1})											−0.11 (0.57)	0.30 (0.10)	0.11 (0.56)
I_D / I_G												0.11 (0.56)	–
I_V / I_G													−0.13 (0.50)

contribution of charcoal and biomass burning-derived particles, as displayed by the significant positive correlation coefficients between TOC and CHAR500 ($r = 0.53$, p-value < 0.01), CHAR250 ($r = 0.50$, p-value < 0.01) and CHAR125 ($r = 0.52$, p-value < 0.01). The pyrogenic source if ROC can be also supported by the correlation coefficient of ROC *vs* CHAR500 ($r = 0.57$, p-value < 0.01), CHAR250 ($r = 0.55$, p-value < 0.01), CHAR125 ($r = 0.61$, p-value < 0.01) and CHAR63 ($r = 0.38$, p-value < 0.05). This evidence is in agreement with the researches of Zethof et al., (2019) that reported ROC as a valuable tool to measure the content of graphitic carbon originated from biomass burning products.

When TOC and ROC are compared to TIC, they display a significant negative correlation ($r = -0.72$, p-value < 0.01; $r = -0.65$, p-value < 0.01, respectively). The behavior of organic and inorganic fractions in soils and sediments is often hardly comprehensible: positive and negative correlations were detected also in similar environmental conditions (Leogrande et al., 2021). Indeed, when the investigated site is a closed system (e.g. a pond or a lake without inflows/outflows), the endogenic input of both TIC and TOC are positively and significantly correlated (Ju et al., 2010). Conversely, in an open system, such as DE deposits, different inputs of TIC and TOC that derive from human activities may have affected the soil conditions. Leogrande et al. (2021) found negative, although not always significant, correlation between TOC and TIC in farms and orchard's soils in the Mediterranean area. The different oxidizing conditions induced by a relatively high concentration of carbonates could have promoted the increase of TIC at the expense of TOC. Other studies proposed that the negative correlation between TOC and TIC can be related to the degradation of organic matter by water dissolution or availability of microorganism able to mineralize the organic matter (Lu et al., 2020). In UDE, the significant negative correlation could be influenced also by the effect of the Ca aggregates, able to stabilize TOC, while CO_2 production can cause a pH decrease, and in turn increase the dissolution of carbonate (Sartori et al., 2007; Shi et al., 2017). The observed negative correlation between TIC and TOC could result from the continuous input of biomass and organic material to the soil, which dilutes the original matrix. The presence of centuries of human activities on the sites of interest could have promoted a process of input of external material and mixing with the original matrix.

The distribution of charcoal particles in the different range sizes are all significant and positively correlated, indicating that such fragments might have the same source. Their exact source is difficult to interpret because of the many processes that could alter charcoal characteristics (e.g., bioturbation, erosion and freezing) (Conedera et al., 2009). A very local source of the signal is suggested by the presence of > 125 μm charcoal (Conedera et al., 2009;Whitlock and Larsen, 2002). However, it cannot be excluded that the significant positive correlation found between charcoal counts per size classes could be ascribed to the fragmentation of larger charcoal particles due to handling processes of soil.

The significant negative correlation between I_V/I_G and the G band position ($r = -0.52$, p-value < 0.01) can be likely associated to graphitization processes as the wavenumber of the G band shift to higher values while I_G increase in intensity (I_V/I_G decreases) when graphitic structures prevails over amorphous ones (Inoue et al., 2017; McDonald-Wharry et al., 2013).

4. Conclusions

From the study of the thin sections, we observed common features and different syn- and post-depositional phenomena responsible for the formation of UDE layers. Our analyses highlight several mechanisms linked to the formation of the base layers of the UDE in the Verona area, primarily the dumping of heterogeneous anthropogenic material combined with the reworking of older sediments. This was further supported by the different radiocarbon dates of the different fractions: the humin fraction gave older dates than the inclusions observed within the UDE (i.e., charcoal). Moreover, one of the aspects resulting from the radiocarbon data is the different information that can be achieved by choosing different organic fractions in cultural layers. In fact the humin fraction suggest the first dwelling of the site, while charcoal dating reveals the period of soil exploitation.

Organic material and charred biomass particles related to backfill (dumping) layers are directly related to human activities, including manufacturing of metal tools and ceramics although these layers are different at different sites. In particular, charcoal and carbon fingerprints of the three sites are different, even when there is proximity in terms of age and location. This proves the occurrence of a horizontal rather than vertical variability of the cultural layers/UDE. This aspect suggests a strong and diversified human influence on these cultural layers. The human influence in terms of massive use of the soil for domestic purposes is further marked by the presence of metallic droplets and trace element concentration (i.e., P, Fe) as well as black burned particles. This points to a process whereby humans affected the natural soil both in VP and SPM. The VP site seems to be situated in the immediate vicinity of artisanal activities (e.g., metal, or ceramic manufacturing), while SPM seems to be more likely affected by the gathering of remains from the close by VP site.

The employment of Raman spectroscopy on charred particles allowed us to account for the various energy-demanding fire uses, these were in agreement with the different ages of the cultural layers. Consistently with predictions based on the samples' dating, the oldest set of samples (collected in the Bronze Age site of Castelar di Leppia) displayed the typical features of more amorphous structures, that express lower carbonization temperatures. In addition, the presence in CDL samples of finer biomass burning residues is explained by the prolonged time of bioturbation (CDL deposit is ca 1500–1800 years older with respect to VP and SPM) highlighted from the observation of the thin sections.

The correlation between the results obtained from different techniques revealed the relation between the most recalcitrant fraction of carbon (ROC) measured in the soil samples and the biomass burning residues collected into the UDE samples. Hence, ROC could be directly associated to past burning activities.

In conclusion, the information inferred from the UDE/cultural layers is extremely local and associated with a sequence of human activities and soil processes specific to particular succession of events, even when the sites are close together. In this scenario, it is necessary to use a statistical approach to connect the aspects of a multi-analytical and multidisciplinary research methodology, necessary to assess the human impact on the surrounding environment in the past.

Declaration of Competing Interest

The authors declare that they have no known competing financial interests or personal relationships that could have appeared to influence the work reported in this paper.

Acknowledgements

This work was supported by the SPIN 2018 InSIDE project, financed by Ca' Foscari University of Venice. The authors would like to thank Elga Lab water, High Wycombe UK for supplying the pure water systems used in this study. Authors would like to thank also Madatec s.r.l (Pessano con Bornago, Italy) for its technical support during Raman analysis.

Appendix A. Supplementary material

Supplementary data to this article can be found online at https://doi.org/10.1016/j.catena.2022.106453.

References

Alexandrovskaya, E.I., Alexandrovskiy, A.L., 2000. History of the cultural layer in Moscow and accumulation of anthropogenic substances in it. Catena 41 (1-3), 249–259.

Alho, C.F.B.V., Samuel-Rosa, A., Martins, G.C., Hiemstra, T., Kuyper, T.W., Teixeira, W. G., 2019. Spatial variation of carbon and nutrients stocks in Amazonian Dark Earth. Geoderma 337, 322–332. https://doi.org/10.1016/j.geoderma.2018.09.040.

Angelini, I., Artioli, G., Nicosia, C., 2017. Metals and metal-working residues. Archaeol. Soil Sediment Micromorphol. 213–222.

Argiriadis, E., Bortolini, M., Kehrwald, N.M., Roman, M., Turetta, C., Hanif, S., Erhenhi, E.O., Ramirez Aliaga, J.M., McWethy, D.B., Myrbo, A.E., Pauchard, A., Barbante, C., Battistel, D., 2021. Rapa Nui (Easter Island) Rano Raraku crater lake basin: Geochemical characterization and implications for the Ahu-Moai Period. PLoS One 16, 1–23. https://doi.org/10.1371/journal.pone.0254793.

ARPAV, 2005. Carta dei suoli del Veneto.

Arroyo-Kalin, M., Neves, E.G., Woods, W.I., 2009. Anthropogenic dark earths of the Central Amazon region: remarks on their evolution and polygenetic composition. Amazonian dark earths: Wim Sombroek's vision. Springer, Dordrecht, pp. 99–125.

Atkinson, C.J., Fitzgerald, J.D., Hipps, N.A., 2010. Potential mechanisms for achieving agricultural benefits from biochar application to temperate soils: A review. Plant Soil 337, 1–18. https://doi.org/10.1007/s11104-010-0464-5.

Babel, U., 1975. Micromorphology of soil organic matter. In: Gieseking, J.E. (Ed.), Soil Components. Springer Berlin Heidelberg, Berlin, Heidelberg, pp. 369–473.

Baldock, J.A., Sanderman, J., MacDonald, L.M., Puccini, A., Hawke, B., Szarvas, S., McGowan, J., 2013. Quantifying the allocation of soil organic carbon to biologically significant fractions. Soil Res. 51, 561–576. https://doi.org/10.1071/SR12374.

Baldock, J.A., Skjemstad, J.O., 2000. Role of the soil matrix and minerals in protecting natural organic materials against biological attack. Org. Geochem. 31, 697–710. https://doi.org/10.1016/S0146-6380(00)00049-8.

Barreto, M.S.C., Elzinga, E.J., Ramlogan, M., Rouff, A.A., Alleoni, L.R.F., 2021. Calcium enhances adsorption and thermal stability of organic compounds on soil minerals. Chem. Geol. 559, 119804 https://doi.org/10.1016/j.chemgeo.2020.119804.

Beckmann, T., 1997. Preparation of thin sections for micromorphological research. Hohenheimer Bodenkundliche Hefte 40, 232.

Bourliva, A., Papadopoulou, L., Aidona, E., 2016. Study of road dust magnetic phases as the main carrier of potentially harmful trace elements. Sci. Total Environ. 553, 380–391. https://doi.org/10.1016/j.scitotenv.2016.02.149.

Bruno, B., Fresco, P., 2014. Verona: archeologia urbana nei negozi del centro storico: lo scavo presso il nuovo store Benetton. Verona Archeol. In: urbana nei negozi del Cent. Stor. lo scavo Press. nuovo store Benett, pp. 103–111.

Butzer, K.W., 2011. Geoarchaeology, climate change, sustainability: A Mediterranean perspective. Geol. Soc. Am. Spec. Pap 201, 1–14.

Butzer, K.W., 2008. Challenges for a cross-disciplinary geoarchaeology: the intersection between environmental history and geomorphology. Geomorphology 101 (1-2), 402–411.

Butzer, K.W., 1982. Archaeology as human ecology: method and theory for a contextual approach. Cambridge University Press.

Cammas, C., 2004. Les "terres noires" urbaines du Nord de la France: première typologie pédosédimentaire. Terres Noires-Dark Earth. Actes la table ronde Int. tenue à Louvain-la-Neuve les 9, 43–55.

Cançado, L.G., Jorio, A., Pimenta, M.A., 2007. Measuring the absolute Raman cross section of nanographites as a function of laser energy and crystallite size. Phys. Rev. B - Condens. Matter Mater. Phys. 76, 1–7. https://doi.org/10.1103/PhysRevB.76.064304.

Cançado, L.G., Takai, K., Enoki, T., Endo, M., Kim, Y.A., Mizusaki, H., Jorio, A., Coelho, L.N., Magalhães-Paniago, R., Pimenta, M.A., 2006. General equation for the determination of the crystallite size la of nanographite by Raman spectroscopy. Appl. Phys. Lett. 88, 1–4. https://doi.org/10.1063/1.2196057.

Canti, M.G., 2017. Charred plant remains. In: Nicosia, C., Stoops, G. (Eds.), Archaeological Soil and Sediment Micromorphology. John Wiley & Sons, pp. 141–142.

Cheng, C.H., Lehmann, J., Engelhard, M.H., 2008. Natural oxidation of black carbon in soils: Changes in molecular form and surface charge along a climosequence. Geochim. Cosmochim. Acta 72, 1598–1610. https://doi.org/10.1016/j.gca.2008.01.010.

Clough, A., Skjemstad, J.O., 2000. Physical and chemical protection of soil organic carbon in three agricultural soils with different contents of calcium carbonate. Soil Res. 38, 1005–1016.

Cohen-Ofri, I., Weiner, L., Boaretto, E., Mintz, G., Weiner, S., 2006. Modern and fossil charcoal: Aspects of structure and diagenesis. J. Archaeol. Sci. 33, 428–439. https://doi.org/10.1016/j.jas.2005.08.008.

Conedera, M., Tinner, W., Neff, C., Meurer, M., Dickens, A.F., Krebs, P., 2009. Reconstructing past fire regimes: methods, applications, and relevance to fire management and conservation. Quat. Sci. Rev. 28, 555–576. https://doi.org/10.1016/j.quascirev.2008.11.005.

Cuesta, A., Dhamelincourt, P., Laureyns, J., Martínez-Alonso, A., Tascón, J.M.D., 1998. Comparative performance of X-ray diffraction and Raman microprobe techniques for the study of carbon materials. J. Mater. Chem. 8, 2875–2879. https://doi.org/10.1039/a805841e.

David, C., 2004. Les «terres noires»: outils méthodologiques, propositions analytiques et perspectives à partir de quelques exemples de sites à «terres noires» de l'Antiquité tardive et du haut Moyen-Age du nord de la France. Verslype L., Brulet R., Dark earth-Terres noires, Actes la table ronde Louvain-la-Neuve, Louvainla-Neuve. Univ. Cathol. Louvain 12–31.

Davidson, D.A., Dercon, G., Stewart, M., Watson, F., 2006. The legacy of past urban waste disposal on local soils. J. Archaeol. Sci. 33, 778–783. https://doi.org/10.1016/j.jas.2005.10.017.

de Sousa, D.V., Guimarães, L.M., Félix, J.F., Ker, J.C., Schaefer, C.E.R.G., Rodet, M.J., Paz-Ferreiro, J., 2020. Dynamic of the structural alteration of biochar in ancient Anthrosol over a long timescale by Raman spectroscopy. PLoS One 15 (3), e0229447.

de Souza, K.W., Lima, H.N., Schaefer, C.E.G.R., Teixeira, W.G., Pulrolnik, K., Corrêa, G. R., 2009. Phosphorous forms in cultivated Indian Black Earth (Anthrosols) of varying texture in the Brazilian Amazon. Rev. Bras. Cienc. do Solo 33, 1347–1355. https://doi.org/10.1590/s0100-06832009000500027.

Dennison, J.R., Holtz, M., 1996. Raman spectroscopy of carbon materials. Spectrosc. (Santa Monica) 11, 38–46.

Devos, Y., 2018. Near total and inorganic phosphorus concentrations as a proxy for identifying ancient activities in urban contexts: The example of dark earth in Brussels, Belgium. Geoarchaeology 33, 470–485. https://doi.org/10.1002/gea.21665.

Devos, Y., Brussel, V.U., Groote, K.D., Agency, F.H., Moens, J., Agency, F.H., Vrydaghs, L., Brussel, V.U., 2019. FACING An interdisciplinary study of. https://doi.org/10.5281/zenodo.3420729.

Devos, Y., Nicosia, C., Vrydaghs, L., Modrie, S., 2013. Studying urban stratigraphy: Dark Earth and a microstratified sequence on the site of the Court of Hoogstraeten (Brussels, Belgium). Integrating archaeopedology and phytolith analysis. Quat. Int. 315, 147–166. https://doi.org/10.1016/j.quaint.2013.07.024.

Devos, Y., Nicosia, C., Vrydaghs, L., Speleers, L., van der Valk, J., Marinova, E., Claes, B., Albert, R.M., Esteban, I., Ball, T.B., Court-Picon, M., Degraeve, A., 2017. An integrated study of Dark Earth from the alluvial valley of the Senne river (Brussels, Belgium). Quat. Int. 460, 175–197. https://doi.org/10.1016/j.quaint.2016.06.025.

Dotterweich, M., Schreg, R., 2019. Archaeonics - (Geo)archaeological studies in anthropogenic dark Earths (ADE) as an example for future-oriented studies of the past. Quat. Int. 502, 309–318. https://doi.org/10.1016/j.quaint.2018.09.026.

Dresselhaus, M.S., Dresselhaus, G., Saito, R., Jorio, A., 2005. Raman spectroscopy of carbon nanotubes. Phys. Rep. 409, 47–99. https://doi.org/10.1016/j.physrep.2004.10.006.

Dubois, N., Jacob, J., 2016. Molecular biomarkers of anthropic impacts in natural archives: a review. Front. Ecol. Evol. 4, 1–16. https://doi.org/10.3389/fevo.2016.00092.

Edmondson, J.L., Stott, I., Potter, J., Lopez-Capel, E., Manning, D.A.C., Gaston, K.J., Leake, J.R., 2015. Black carbon contribution to organic carbon stocks in urban soil. Environ. Sci. Technol. 49, 8339–8346. https://doi.org/10.1021/acs.est.5b00313.

Enache, M.D., Cumming, B.F., 2006. Tracking recorded fires using charcoal morphology from the sedimentary sequence of Prosser Lake, British Columbia (Canada). Quat. Res. 65, 282–292. https://doi.org/10.1016/j.yqres.2005.09.003.

Ferrari, A.C., Robertson, J., 2000. Interpretation of Raman spectra of disordered and amorphous carbon. Phys. Rev. B - Condens. Matter Mater. Phys. 61, 14095–14107. https://doi.org/10.1103/PhysRevB.61.14095.

Ferrari, A.C., Robertson, J., 2004. Raman spectroscopy of amorphous, nanostructured, diamond-like carbon, and nanodiamond. Philosophical Transactions of the Royal Society of London. Series A: Mathematical, Physical and Engineering Sciences 362 (1824), 2477–2512. https://doi.org/10.1098/rsta.2004.1452.

Fisher, G.L., Prentice, B.A., Sllberman, D., Ondov, J.M., Biermann, A.H., Ragainl, R.C., McFarl, A.R., 1978. Physical and morphological studies of size-classified coal fly ash. Environ. Sci. Technol. 12, 447–451. https://doi.org/10.1021/es60140a008.

Galinié, H., 2007. L'expression terres noires, un concept d'attente. Les petits Cah. d'Anatole 15.

Glaser, B., Balashov, E., Haumaier, L., Guggenberger, G., Zech, W., 2000. Black carbon in density fractions of anthropogenic soils of the brazilian amazon region. Org. Geochem. 31 (7-8), 669–678.

Glaser, B., Birk, J.J., 2012. State of the scientific knowledge on properties and genesis of anthropogenic dark earths in central amazonia (terra preta de índio). Geochim. Cosmochim. Acta 82, 39–51. https://doi.org/10.1016/j.gca.2010.11.029.

Glaser, B., Haumaier, L., Guggenberger, G., Zech, W., 2001. The "Terra Preta" phenomenon: a model for sustainable agriculture in the humid tropics. Naturwissenschaften 88, 37–41. https://doi.org/10.1007/s001140000193.

Glikson, A., 2013. Fire and human evolution: the deep-time blueprints of the Anthropocene. Anthropocene 3, 89–92. https://doi.org/10.1016/j.ancene.2014.02.002.

Hardy, B., Cornelis, J.T., Houben, D., Leifeld, J., Lambert, R., Dufey, J.E., 2017. Evaluation of the long-term effect of biochar on properties of temperate agricultural soil at pre-industrial charcoal kiln sites in Wallonia. Belgium. Eur. J. Soil Sci. 68, 80–89. https://doi.org/10.1111/ejss.12395.

Hernandez-Soriano, M.C., Kerré, B., Goos, P., Hardy, B., Dufey, J., Smolders, E., 2016. Long-term effect of biochar on the stabilization of recent carbon: soils with historical inputs of charcoal. GCB Bioenergy 8, 371–381. https://doi.org/10.1111/gcbb.12250.

Hobley, E., Willgoose, G.R., Frisia, S., Jacobsen, G., 2013. Environmental and site factors controlling the vertical distribution and radiocarbon ages of organic carbon in a sandy soil. Biol. Fertil. Soils 49, 1015–1026. https://doi.org/10.1007/s00374-013-0800-z.

Hobley, E.U., Baldock, J., Wilson, B., 2016. Environmental and human influences on organic carbon fractions down the soil profile. Agric. Ecosyst. Environ. 223, 152–166. https://doi.org/10.1016/j.agee.2016.03.004.

Howard, J.L., Orlicki, K.M., 2016. Composition, micromorphology and distribution of microartifacts in anthropogenic soils, Detroit, Michigan, USA. Catena 138, 103–116. https://doi.org/10.1016/j.catena.2015.11.016.

Inoue, J., Yoshie, A., Tanaka, T., Onji, T., Inoue, Y., 2017. Disappearance and alteration process of charcoal fragments in cumulative soils studied using Raman spectroscopy. Geoderma 285, 164–172. https://doi.org/10.1016/j.geoderma.2016.09.032.
Ishimaru, K., Hata, T., Bronsveld, P., Meier, D., Imamura, Y., 2007. Spectroscopic analysis of carbonization behavior of wood, cellulose and lignin. J. Mater. Sci. 42, 122–129. https://doi.org/10.1007/s10853-006-1042-3.
Jawhari, T., Roid, A., Casado, J., 1995. Raman spectroscopic characterization of some commercially available carbon black materials. Carbon N. Y. 33, 1561–1565. https://doi.org/10.1016/0008-6223(95)00117-V.
Jeffery, S., Verheijen, F.G.A., van der Velde, M., Bastos, A.C., 2011. A quantitative review of the effects of biochar application to soils on crop productivity using meta-analysis. Agric. Ecosyst. Environ. 144, 175–187. https://doi.org/10.1016/j.agee.2011.08.015.
Jorio, A., Ribeiro-Soares, J., Cançado, L.G., Falcão, N.P.S., Dos Santos, H.F., Baptista, D. L., Martins Ferreira, E.H., Archanjo, B.S., Achete, C.A., 2012. Microscopy and spectroscopy analysis of carbon nanostructures in highly fertile Amazonian anthrosoils. Soil Tillage Res. 122, 61–66. https://doi.org/10.1016/j.still.2012.02.009.
Ju, J., Zhu, L.-P., Wang, J., Xie, M., Zhen, X., Wang, Y., Peng, P., 2010. Water and sediment chemistry of Lake Pumayum Co, South Tibet, China: Implications for interpreting sediment carbonate. J. Paleolimnol. 43 (3), 463–474.
Kawakami, M., Karato, T., Takenaka, T., Yokoyama, S., 2005. Structure analysis of coke, wood charcoal and bamboo charcoal by Raman spectroscopy and their reaction rate with CO2. ISIJ Int. 45, 1027–1034. https://doi.org/10.2355/isijinternational.45.1027.
Kern, D.C., Lima, H.P., da Costa, J.A., de Lima, H.V., Browne Ribeiro, A., Moraes, B.M., Kämpf, N., 2017. Terras pretas: approaches to formation processes in a new paradigm. Geoarchaeology 32, 694–706. https://doi.org/10.1002/gea.21647.
Kirchgeorg, T., Schüpbach, S., Kehrwald, N., McWethy, D.B., Barbante, C., 2014. Method for the determination of specific molecular markers of biomass burning in lake sediments. Org. Geochem. 71, 1–6. https://doi.org/10.1016/j.orggeochem.2014.02.014.
Lambrecht, G., Rodríguez de Vera, C., Jambrina-Enríquez, M., Crevecoeur, I., Gonzalez-Urquijo, J., Lazuen, T., Monnier, G., Pajović, G., Tostevin, G., Mallol, C., 2021. Characterisation of charred organic matter in micromorphological thin sections by means of Raman spectroscopy. Archaeol. Anthropol. Sci. 13 https://doi.org/10.1007/s12520-020-01263-3.
Lehmann, A., Stahr, K., 2007. Nature and significance of anthropogenic urban soils. J. Soils Sediments 7, 247–260. https://doi.org/10.1065/jss2007.06.235.
Leogrande, R., Vitti, C., Castellini, M., Mastrangelo, M., Pedrero, F., Vivaldi, G.A., Stellacci, A.M., 2021. Comparison of two methods for total inorganic carbon estimation in three soil types in mediterranean area. Land 10, 1–11. https://doi.org/10.3390/land10040409.
Liang, B., Lehmann, J., Sohi, S.P., Thies, J.E., O'Neill, B., Trujillo, L., Gaunt, J., Solomon, D., Grossman, J., Neves, E.G., Luizão, F.J., 2010. Black carbon affects the cycling of non-black carbon in soil. Org. Geochem. 41, 206–213. https://doi.org/10.1016/j.orggeochem.2009.09.007.
Lu, T., Wang, X., Zhang, W., 2020. Total and dissolved soil organic and inorganic carbon and their relationships in typical loess cropland of Fengu Basin. Geosci. Lett. 7 https://doi.org/10.1186/s40562-020-00167-3.
Macedo, R.S., Teixeira, W.G., Corrêa, M.M., Martins, G.C., Vidal-Torrado, P., Paz-Ferreiro, J., 2017. Pedogenetic processes in anthrosols with pretic horizon (amazonian dark earth) in central amazon, brazil. PLoS One 12 (5), e0178038.
Macphail, R., Linderholm, J., 2004. Dark earth": recent studies of" Dark earth" and" dark-earth-like. microstratigraphy in England, UK.
Macphail, R.I., 1994. The reworking of urban stratigraphy by human and natural processes. Urban-rural connexions Perspect. from Environ. Archaeol. 13–43.
Macphail, R.I., 1981. Soil and botanical studies of the "Dark Earth," in: Jones, M.., Dimbleby, G.W. (Eds.), The Environment of Man: The Iron Age to the Anglo-Saxon Period. Oxford, pp. 309–331.
McDonald-Wharry, J., Manley-Harris, M., Pickering, K., 2013. Carbonisation of biomass-derived chars and the thermal reduction of a graphene oxide sample studied using Raman spectroscopy. Carbon N. Y. 59, 383–405. https://doi.org/10.1016/j.carbon.2013.03.033.
Migliavacca, M., Pizzeghello, D., Ertani, A., Nardi, S., 2013. Chemical analyses of archaeological sediments identified the ancient activity areas of an Iron age building at Rotzo (Vicenza, Italy). Quat. Int. 289, 101–112. https://doi.org/10.1016/j.quaint.2012.07.016.
Mustaphi, C.J.C., Pisaric, M.F.J., 2014. A classification for macroscopic charcoal morphologies found in Holocene lacustrine sediments. Prog. Phys. Geogr. 38, 734–754. https://doi.org/10.1177/0309133314548886.
Natali, C., Bianchini, G., Carlino, P., 2020. Thermal stability of soil carbon pools: Inferences on soil nature and evolution. Thermochim. Acta 683, 178478. https://doi.org/10.1016/j.tca.2019.178478.
Neves, E.G., Petersen, J.B., Robert, N., Augusto, C., Silva, D.A., 2003. Amazonian Dark Earths. Amaz. Dark Earths. https://doi.org/10.1007/1-4020-2597-1.
Ngu, L.N., Wu, H., Zhang, D.K., 2007. Characterisation of cenospheres in fly ash from Australian power stations. 6th Asia-Pacific Conf. Combust. ASPACC 2007 31, 3437–3445.
Nicosia, C., 2018. DELLE STRATIFICAZIONI URBANE POST-CLASSICHE.
Nicosia, C., Devos, Y., 2014. Urban dark earth. In: Smith, C. (Ed.), Encyclopedia of Global Archaeology. Springer New York, New York, NY, pp. 7532–7540.
Nicosia, C., Devos, Y., Macphail, R.I., 2017. European dark earth. Archaeol. soil sediment Micromorphol. 331–343.
Nicosia, C., Ertani, A., Vianello, A., Nardi, S., Brogiolo, G.P., Chavarría Arnau, A., Becherini, F., 2019. Heart of darkness: an interdisciplinary investigation of the urban anthropic deposits of the Baptistery of Padua (Italy). Archaeol. Anthropol. Sci. 11, 1977–1993. https://doi.org/10.1007/s12520-018-0646-2.
Nicosia, C., Langohr, R., Mees, F., Arnoldus-Huyzendveld, A., Bruttini, J., Cantini, F., 2012. Medieval dark earth in an active alluvial setting from the uffizi gallery complex in florence, italy. Geoarchaeology 27, 105–122. https://doi.org/10.1002/gea.21403.
Paetsch, L., Mueller, C.W., Rumpel, C., Angst, Š., Wiesheu, A.C., Girardin, C., Ivleva, N.P., Niessner, R., Kögel-Knabner, I., 2017. A multi-technique approach to assess the fate of biochar in soil and to quantify its effect on soil organic matter composition. Org. Geochem. 112, 177–186. https://doi.org/10.1016/j.orggeochem.2017.06.012.
Patten, H.V., Meadows, K.E., Hutton, L.A., Iacobini, J.G., Battistel, D., McKelvey, K., Colburn, A.W., Newton, M.E., MacPherson, J.V., Unwin, P.R., 2012. Electrochemical mapping reveals direct correlation between heterogeneous electron-transfer kinetics and local density of states in diamond electrodes. Angew. Chemie - Int. Ed. 51, 7002–7006. https://doi.org/10.1002/anie.201203057.
Pessenda, L.C.R., Gouveia, S.E.M., Aravena, R., 2001. Radiocarbon Dating of Total Soil Organic Matter and Humin Fraction and Its Comparison with 14 C Ages of Fossil Charcoal. Radiocarbon dating of total soil organic matter and humin fraction and its comparison with 14C ages of fossil charcoal 43 (2B), 595–601.
Pignatello, J.J., Kwon, S., Lu, Y., 2006. Effect of natural organic substances on the surface and adsorptive properties of environmental black carbon (Char): attenuation of surface activity by humic and fulvic acids. Environ. Sci. Technol. 40, 7757–7763. https://doi.org/10.1021/es061307m.
Qi, F., Naidu, R., Bolan, N.S., Dong, Z., Yan, Y., Lamb, D., Bucheli, T.D., Choppala, G., Duan, L., Semple, K.T., 2017. Pyrogenic carbon in Australian soils. Sci. Total Environ. 586, 849–857. https://doi.org/10.1016/j.scitotenv.2017.02.064.
Reimann, C., De Caritat, P., 2000. Intrinsic flaws of element enrichment factors (EFs) in environmental geochemistry. Environ. Sci. Technol. 34, 5084–5091. https://doi.org/10.1021/es001339o.
Ribeiro-Soares, J., Cançado, L.G., Falcão, N.P.S., Martins Ferreira, E.H., Achete, C.A., Jorio, A., 2013. The use of raman spectroscopy to characterize the carbon materials found in amazonian anthrosoils. J. Raman Spectrosc. 44, 283–289. https://doi.org/10.1002/jrs.4191.
Rowley, M.C., Grand, S., Verrecchia, É.P., 2018. Calcium-mediated stabilisation of soil organic carbon. Biogeochemistry 137, 27–49. https://doi.org/10.1007/s10533-017-0410-1.
Rumpel, C., Leifeld, J., Santin, C., Doerr, S., 2015. Movement of biochar in the environment, in: Biochar for Environmental Management. Routledge, p. 18.
Salzani, L., 1983. Castellar di leppia (Lavagno). Bollettino Del Museo Civico Di Storia Naturale Di Verona. 518–521.
Sartori, F., Lal, R., Ebinger, M.H., Eaton, J.A., 2007. Changes in soil carbon and nutrient pools along a chronosequence of poplar plantations in the columbia plateau, oregon. USA. Agric. Ecosyst. Environ. 122, 325–339. https://doi.org/10.1016/j.agee.2007.01.026.
Schmidt, M., 2013. Amazonian dark earths: pathways to sustainable development in tropical rainforests? Bol. do Mus. Para. Emilio GoeldiCiencias Humanas 8, 11–38. https://doi.org/10.1590/S1981-81222013000100002.
Schmidt, M.J., Rapp Py-Daniel, A., de Paula Moraes, C., Valle, R.B.M., Caromano, C.F., Texeira, W.G., Barbosa, C.A., Fonseca, J.A., Magalhães, M.P., Silva do Carmo Santos, D., da Silva e Silva, R., Guapindaia, V.L., Moraes, B., Lima, H.P., Neves, E.G., Heckenberger, M.J., 2014. Dark earths and the human built landscape in amazonia: a widespread pattern of anthrosol formation. J. Archaeol. Sci. 42, 152–165.
Schmidt, M.W.I., Noack, A.G., Osmond, G., 2000. Analysis, distribution, implications, and current challenges 14, 777–793.
Schmidt, M.W.I., Skjemstad, J.O., Jäger, C., 2002. Carbon isotope geochemistry and nanomorphology of soil black carbon: black chernozemic soils in central Europe originate from ancient biomass burning. Global Biogeochem. Cycles 16 (4), 70-1–70-8.
Shi, H.J., Wang, X.J., Zhao, Y.J., Xu, M.G., Li, D.W., Guo, Y., 2017. Relationship between soil inorganic carbon and organic carbon in the wheat-maize cropland of the north china plain. Plant Soil 418, 423–436. https://doi.org/10.1007/s11104-017-3310-1.
Silva, L.C.R., Corrêa, R.S., Wright, J.L., Bomfim, B., Hendricks, L., Gavin, D.G., Muniz, A. W., Martins, G.C., Motta, A.C.V., Barbosa, J.Z., Melo, V.d.F., Young, S.D., Broadley, M.R., Santos, R.V., 2021. A new hypothesis for the origin of amazonian Dark Earths. Nat. Commun. 12 (1) https://doi.org/10.1038/s41467-020-20184-2.
Smidt, E., Tintner, J., Klemm, S., Scholz, U., 2017. FT-IR spectral and thermal characterization of ancient charcoals - a tool to support archeological and historical data interpretation. Quat. Int. 457, 43–49. https://doi.org/10.1016/j.quaint.2016.11.031.
Smidt, E., Tintner, J., Nelle, O., Oliveira, R.R., Patzlaff, R., Novotny, E.H., Klemm, S., 2020. Infrared spectroscopy refines chronological assessment, depositional environment and pyrolysis conditions of archeological charcoals. Sci. Rep. 10, 1–11. https://doi.org/10.1038/s41598-020-69445-6.
Steiner, C., Teixeira, W.G., Lehmann, J., Nehls, T., De MacÊdo, J.L.V., Blum, W.E.H., Zech, W., 2007. Long term effects of manure, charcoal and mineral fertilization on crop production and fertility on a highly weathered Central Amazonian upland soil. Plant Soil 291, 275–290. https://doi.org/10.1007/s11104-007-9193-9.
Stoops, G., 2003. Guidelines for analysis and description of soil and regolith thin sections. Soil Sci. Soc. Am., Madison, WI.
Sukopp, H., 1979. The soil, flora, and vegetation of Berlin's waste lands.
Sutherland, R.A., 2000. Bed sediment-associated trace metals in an urban stream, Oahu. Hawaii. Environ. Geol. 39, 611–627. https://doi.org/10.1007/s002540050473.
Theurer, T., Muirhead, D.K., Jolley, D., Mauquoy, D., 2021. The applicability of raman spectroscopy in the assessment of palaeowildfire intensity. Palaeogeogr. Palaeoclimatol. Palaeoecol. 570, 110363 https://doi.org/10.1016/j.palaeo.2021.110363.

Tinti, A., Tugnoli, V., Bonora, S., Francioso, O., 2015. Recent applications of vibrational mid-infrared (IR) spectroscopy for studying soil components: a review. J. Cent. Eur. Agric. 16, 1–22. https://doi.org/10.5513/JCEA01/16.1.1535.

Trumbore, S.E., 1997. Potential responses of soil organic carbon to global environmental change. Proc. Natl. Acad. Sci. U. S. A. 94, 8284–8291. https://doi.org/10.1073/pnas.94.16.8284.

Tuinstra, F., Koenig, J., 1970. Raman spectrum of graphite. J. Chem. Phys. 53, 1126–1130. https://doi.org/10.1063/1.1674108.

Valladares, G.S., Pereira, M.G., Anjos, L.H.C.D., Benites, V.D.M., Ebeling, A.G., Mouta, R. D.O., 2007. Humic substance fractions and attributes of histosols and related high-organic-matter soils from Brazil. Commun. Soil Sci. Plant Anal. 38, 763–777. https://doi.org/10.1080/00103620701220759.

van der Plicht, J., Streurman, H.J., van Mourik, J.M., 2019. Radiocarbon dating of soil archives. Developments in Quaternary Sci. https://doi.org/10.1016/B978-0-444-64108-3.00003-3.

van Mourik, J.M., Seijmonsbergen, A.C., Slotboom, R.T., Wallinga, J., 2012. Impact of human land use on soils and landforms in cultural landscapes on aeolian sandy substrates (Maashorst, SE-Netherlands). Quat. Int. 265, 74–89. https://doi.org/10.1016/j.quaint.2011.06.053.

Vittori Antisari, L., Cremonini, S., Desantis, P., Calastri, C., Vianello, G., 2013. Chemical characterisation of anthro-technosols from Bronze to Middle Age in Bologna (Italy). J. Archaeol. Sci. 40, 3660–3671. https://doi.org/10.1016/j.jas.2013.04.023.

Vrydaghs, L., Ball, T.B., Devos, Y., 2016. Beyond redundancy and multiplicity. integrating phytolith analysis and micromorphology to the study of brussels dark earth. J. Archaeol. Sci. 68, 79–88. https://doi.org/10.1016/j.jas.2015.09.004.

Wang, Y., Alsmeyer, D.C., McCreery, R.L., 1990. Raman spectroscopy of carbon materials: structural basis of observed spectra. Chem. Mater. 2, 557–563. https://doi.org/10.1021/cm00011a018.

Whitlock, C., Higuera, P.E., McWethy, D.B., Briles, C.E., 2010. Paleoecological perspectives on fire ecology: revisiting the fire-regime concept~!2009-09-02~!2009-11-09~!2010-03-05~! Open Ecol. J. 3, 6–23. https://doi.org/10.2174/1874213001003020006.

Whitlock, C., Larsen, C., 2002. Charcoal as a Fire Proxy 75–97. https://doi.org/10.1007/0-306-47668-1_5.

Wiedner, K., Schneeweiß, J., Dippold, M.A., Glaser, B., 2015. Anthropogenic dark earth in northern germany - the nordic analogue to terra preta de índio in amazonia. Catena 132, 114–125. https://doi.org/10.1016/j.catena.2014.10.024.

Wilson, C.A., Davidson, D.A., Cresser, M.S., 2008. Multi-element soil analysis: an assessment of its potential as an aid to archaeological interpretation. J. Archaeol. Sci. 35, 412–424. https://doi.org/10.1016/j.jas.2007.04.006.

Woods, W.I., McCann, J.M., 1999. The anthropogenic origin and persistence of Amazonian dark earths. Conf. Lat. Am. Geogr. Yearb. 25, 7–14.

Wouters, B., Devos, Y., Milek, K., Vrydaghs, L., Bartholomieux, B., Tys, D., Moolhuizen, C., van Asch, N., 2017. Medieval markets: A soil micromorphological and archaeobotanical study of the urban stratigraphy of Lier (Belgium). Quat. Int. 460, 48–64. https://doi.org/10.1016/j.quaint.2017.03.002.

Zamanian, K., Pustovoytov, K., Kuzyakov, Y., 2016. Pedogenic carbonates: Forms and formation processes. Earth-Science Rev. 157, 1–17. https://doi.org/10.1016/j.earscirev.2016.03.003.

Zethof, J.H.T., Leue, M., Vogel, C., Stoner, S.W., Kalbitz, K., 2019. Identifying and quantifying geogenic organic carbon in soils - the case of graphite. Soil 5, 383–398. https://doi.org/10.5194/soil-5-383-2019.